Electrical studies of Fe-related defect complexes in silicon

Chi Kwong Tang

Semiconductor Physics
Department of Physics
Faculty of Mathematics and Natural Sciences
University of Oslo

A thesis submitted for the degree of

Philosophiae Doctor (Ph.D.)

2012 September

Series of dissertations submitted to the
Faculty of Mathematics and Natural Sciences, University of Oslo
No. 1285

ISSN 1501-7710

Cover: Inger Sandved Anfinsen.
Printed in Norway: AIT Oslo AS.

Produced in co-operation with Akademika publishing.
The thesis is produced by Akademika publishing merely in connection with the thesis defence. Kindly direct all inquiries regarding the thesis to the copyright holder or the unit which grants the doctorate.

Abstract

Iron (Fe) is an important impurity in solar-grade silicon which contributes substantially in degrading the efficiency of solar cells. The degradation is mainly caused by the Fe atoms situating at an unperturbed tetrahedral interstitial sites (Fe_i) in the silicon crystal, consequently acting as a recombination center. By altering the position and the neighbouring environment at which the Fe atoms reside, there are opportunities in minimizing or neutralizing the electrical activity of Fe. Furthermore, utilizing the high mobility of Fe, one can increase the performance of a device by accumulating the Fe atoms from critical regions into regions where Fe can be tolerated. These approaches can help in realizing high efficient solar cells based on cheap and highly Fe-contaminated silicon. In this work, we have investigated the interaction between Fe and defects relevant to solar cells, using mainly electrical characterization methods such as capacitance-voltage measurement, deep level transient spectroscopy and admittance spectroscopy.

From the study of potential hydrogen passivation of Fe, hydrogen was introduced through wet chemical etching and further driven to a defined region. Using depth profiles, it is found that incorporation of hydrogen stimulates the dissociation of the iron-boron (Fe-B) pair, releasing and resulting in the unwanted Fe_i. At the same time, no passivation of Fe by hydrogen has been observed.

On the investigation of the mechanism of phosphorus gettering of metal impurities, vacancies have been generated through proton-irradiation. The resulting irradiation-induced defects were examined for reactions with Fe after heat treatments. Based on the evolution of defect concentrations by isochronal annealings, it is found that Fe interacts with the divacancy and

the vacancy-oxygen complexes, forming deep levels of 0.28 eV and 0.34 eV above the valence band edge (E_V), respectively.

In the search for substitutional Fe to investigate its electrical activity and thermal stability, measurements were performed around the projected range of Fe-implantations after rapid thermal annealing. A shallow acceptor is uncovered with an energy level position of E_V+0.06 eV and a defect concentration closely following the calculated concentration of the Fe-implantation dose. However, chemical analysis with secondary ion-mass spectrometry shows out-diffusion of Fe from the region around the projected range after annealing. This suggests that the formation of the shallow acceptor is only assisted/promoted by Fe without Fe being a part of the final complex.

Acknowledgements

This work is completed with the help of many amazing people providing their share of support, encouragement and guidance. I would like to give my greatest gratitude to my supervisors. Firstly, a thanks to my main supervisor Prof. Edouard Monakhov for giving me the opportunity to become a PhD candidate and for patiently guiding me through the many research and scientific problems, and, at the same time, providing me with many healthy challenges. This has generated much unexpected joy in completing this work. Secondly, a thanks to my co-supervisor Dr. Lasse Vines for all the technical help, discussions and idea sharing which has shown me the many different point of views of an experiment. Thirdly, a thanks to my co-supervisor Prof. Bengt Gunnar Svensson for securing the high quality of the works, both in the scientific and grammatic content.

Our technicians, Viktor Bobal and Stig Bengt Mikael Sjödin, deserve a huge thanks for making sure that equipments are up and running. Furthermore, a special thanks to Viktor for performing all the ion-implantations which have enabled many of my experiments. Your effort is highly appreciated.

Friends and collogues at MiNaLab (now LENS, Light and Electricity from Novel Semiconductors), of course, play a significant role in the support and motivation during the PhD period. An immense thanks to Helge Malmbekk, Vincent Quemener, Lars Løvlie, Knut Erik Knutsen, Mareike Trunk, Esben Lund, Hans Bjørge Normann, Klaus Magnus Håland Johansen, Per Filip Lindberg, Naveengoud Ganagona, Ramón Schifano, Janicke Furberg, Ethan Schuyler Long, Paul Henrich Michael Böttger and Bahman Raeissi for creating a good working environment, taking up interesting discussions and bringing all the delicious cakes.

A thanks must also be given to my collegues outside LENS for discussions, helping and giving me access to their equipments. These collegues are Marie Syre Wiig, Halvard Haug, Tine Uberg Nærland, Smagul Karazhanov, Jeyanthinath Mayandi, Arve Holt and Erik Marstein.

Outside work place, there are friends who deserve a thanks for the good times and for the patience of listening to what my work is about. Further, a thanks to Yi Ji for creating many memorable moments in my life and many exciting food.

Finally, my parents (Sui Hing Chow and Kwok Wah Tang), sister (Ivy Tsz Kwan Tang) and brother (Chi Ko Tang) have been both supportive and inspirational in my life. This has not only relieved much stress during the Ph.D. period but also given me much motivation to complete the degree. Thank you all!

With no doubt in my young and hungry mind, I am glad that I have spend three years of my life in completing my PhD degree at LENS which has enriched my knowledge and widen my horizon.

Contents

List of Articles

I **Electrically active centers introduced in p-type Si by rapid thermal processing. C.K. Tang, E. Lund, E.V. Monakhov, J. Mayandi, A. Holt and B.G. Svensson.** ***Phys. Status Solidi C 8, No. 3, 725-728 (2011)***

II **Hydrogen-induced dissociation of the Fe-B pair in boron-doped p-type silicon. C.K. Tang, L. Vines, B.G. Svensson and E.V. Monakhov.** ***Solid State Phenomena. Vol. 178-179, 183-187 (2011)***

III **Interaction between hydrogen and the Fe-B pair in boron-doped p-type silicon. C.K. Tang, L. Vines, B.G. Svensson and E.V. Monakhov.** ***Appl. Phys. Lett. 99, 052106 (2011)***

IV **Deep level transient spectroscopy on proton-irradiated Fe-contaminated p-type silicon. C.K. Tang, L. Vines, B.G. Svensson and E.V. Monakhov.** ***Phys. Status Solidi C, In production (2012)***

V **Divacancy-iron complexes in silicon. C.K. Tang, L. Vines, V. P. Markevich, B.G. Svensson and E.V. Monakhov.** ***Submitted to Journal of Applied Physics (2012)***

VI **Iron-assisted formation of a shallow acceptor in p-type silicon. C.K. Tang, L. Vines, B.G. Svensson and E.V. Monakhov.** ***Submitted to Phys. Status Solidi B (2012)***

Chapter 1

Introduction

Silicon has been the dominant semiconductor material for more than half a century and intensively studied. This has given silicon an advantage as a material for solar cells where more than 80% of the market is based on crystalline silicon (1). Single crystalline and multicrystalline silicon are the main ones used and they differ generally by quality and cost. Multicrystalline silicon contains higher impurity concentration due to in-diffused metal during growth, and the impurities can easily form precipitates at grain boundaries (2, 3). These precipitates can degrade a solar cell by increasing the leakage current and increasing the probability of shunting. Moreover, the precipitates can also be dissolved during high temperature processing of a solar cell, producing point defects with strongly degrading effects, even at low concentrations (4, 5). Among the metal impurities, transition metals such as iron (Fe), are particularly detrimental for the solar cell and integrated circuit performance. Solar cells based on single crystalline silicon will degrade similarly when contaminated with the metals.

The study of Fe in Si began already in 1956 (6) and is one of the most studied transition metals in silicon (7, 8). More than 30 Fe-related defects have been uncovered using electron paramagnetic resonance (EPR) and around 12 electrically active defects are firmly reported using electrical characterization methods. However, only 4 of the electrically active defects are relevant for boron-doped silicon which is mainly used for solar cells. Two of the defects are well-known for their degradation characteristics in commercial silicon-based solar cells, and they are the interstitial Fe (Fe_i) and the Fe-B pair (consisting of an interstitial Fe next to a substitutional boron (B)) (9). These

two defects are reversibly interchangeable and the dissociation of the Fe-B pair into the Fe_i leads to a degradation of the solar cell. Such dissociation can be initiated by heat treatment, minority carrier injection or illumination(10, 11), where the latter one is the so-called light-induced degradation (LID). Interestingly, having $5\times10^{22}cm^{-3}$ of silicon atoms in a crystal, a significant degradation can already be observed with a concentration of Fe_i of $1\times10^{12}cm^{-3}$ (12). Large amount of research has been focused on reducing the concentration of electrically active Fe, by, for instance, accumulating Fe in a non-affecting region (gettering) or forming Fe-related complexes which are electrically in-active (passivation).

The principle of gettering is to create a spatial region capable of capturing a large amount of Fe by forming stable complexes. The gettering process can occur with, for instance, oxygen precipitates (13), structural damage (14), electrically charged regions (15) or phosphorus in-diffusion (16). The latter method is essentially one of the steps in forming standard solar cells and, therefore, provide rinsing of the material "for free". However, the phosphorus gettering process is not well understood in terms of the underlying defect reactions which sets limitations on the optimization of the gettering process. Thus, it is important to gain further understanding in the defects reactions with Fe.

Passivation of defects is commonly performed with hydrogen, as illustrated by the many reports showing its capability on vacancies (17), dangling bonds (18), grain boundaries (19, 20) and dopants (21). For that reason, introduction of hydrogen is often an integrated process in the production of solar cells and efficiency improvements have been observed. However, reports have also shown that reactions between H and transition metals can form electrically active defects such as Au-H (22), Pt-H (23) and Ag-H (24). In the case of Fe, experimental reports on the effect of H on Fe are scarce and contradicting (25, 26, 27) which demands further examinations. Fortunately, theoretical estimates have been performed recently to predict the stability and the electrical activity of possible Fe-H complexes (28, 29), but the predictions still require experimental verifications.

In the work of this thesis, Fe has been introduced in silicon under various conditions and investigated for Fe-related complexes using electrical characterization techniques. The origin, formation and stability of Fe-related complexes are discussed.

This thesis is organized into four chapters. Chapter 2 introduces the basic semiconductor concepts and physics which assist in the understanding of the electrical characterization techniques used and the purposes of the experiments. Chapter 3 describes the electrical characterization techniques, and Chapter 4 summarizes the work in the manuscripts and published articles.

Chapter 2

Basic semiconductor concepts and physics

This chapter introduces the basic concepts of semiconductor physics and will aid in the understanding of this thesis. Detailed concepts which are closely related to a subject, however, will only be briefly mentioned and references are given for those interested.

2.1 Schottky barrier contact

The Schottky barrier contact (SBC) is an important diode structure, formed between a semiconductor and an appropriate metal (30). A diode exhibits a non-linear current-voltage characteristics, and it can be understood by considering the energy potentials and the charge carrier distribution of the system, based on the Schottky-Mott limit (31). Figure 2.1a shows schematically a system consisting of a metal, for instance aluminium, and a semiconductor, for instance p-type silicon, in a non-interacting distance where energy potentials are situated relative to the vacuum level (E_{vac}). In the Si, electrons and holes (quasi-particle with opposite charge state of the electron) occupy energy levels in the conduction band and the valence band, respectively. These bands are seperated by a band gap (E_G) which is intrinsically free of energy levels, and the gap distance is controlled by the conduction band edge (E_C) and the valence band edge (E_V). The amount of electrons and holes in the respective bands are expressed by the Fermi-level

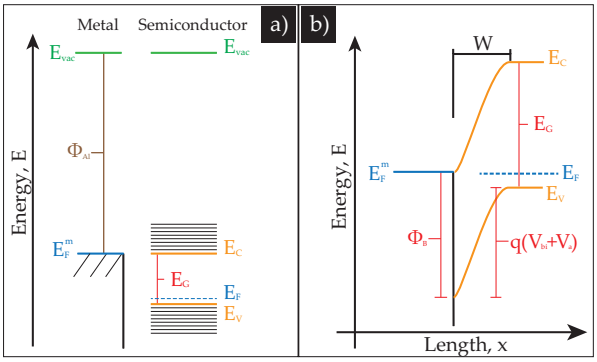

Figure 2.1: Schematics of energy potentials for a system of Al and p-type Si at a) non-interacting distance and b) in direct contact.

(E_F) and are exponentially dependent on the position of the E_F. In a semiconductor where the current is dominated by electrons, that is an n-type material, the Fermi-level is found close to the E_C, while the opposite is true for a p-type semiconductor.

Figure 2.1b shows a simplified schematic of the Al and the Si in direct contact. The Fermi-levels in Fig.2.1a is aligned due to diffusion of free charge carriers (holes, in this case) across the junction, leaving ionized dopants and giving rise to an electrical field which opposes the diffusion. This results in a region depleted of free charge carrier, called the depletion region (W), and the electrical field results in a built-in potential (V_{bi}). The V_{bi} multiplied by the elementary charge[1], q, describes the energy barrier the free charge carriers must surmount in order to reach the metal from the semiconductor when no external voltage is applied. This energy barrier can be manipulated by simply applying a voltage (V_a) across the system. In a forward bias voltage, the energy barrier is decreased and the amount of charge carriers moving from the semiconductor to the metal increases exponentially, resulting in an exponential increase in the current density. While in a reverse bias voltage, the current density is affected by Φ_B, which is determined by the choice of metal, and the amount of minority carriers (electrons, in the case of Fig.2.1b) in the semiconductor. Another direct consequence of applying a voltage over a diode is that the width of the depletion region changes, where W can

[1] $q \simeq 1.602 \times 10^{-19}\, C$

be expressed as

$$W_{Schottky} = \sqrt{\frac{2\epsilon_0\epsilon_r}{qN_{a/d}}\left(V_{bi} + V_a - \frac{kT}{q}\right)}, \tag{2.1}$$

where ϵ_0 is the permittivity of free space[1], ϵ_r is the relative permittivity of the semiconductor, $N_{a/d}$ is the doping concentration of acceptors/donors, k is the Boltzmann constant[2] and T is the absolute temperature.

Another important diode structure is the pn-junction where *one* material is doped p-type in one region and n-type in the neighbouring region, creating a difference in the Fermi-levels between the n-type and the p-type region (30). This difference results, again, in the diffusion of free charge carrier across the junction, producing the energy barrier and the depletion region that can be expressed as

$$W_{pn} = \sqrt{\frac{2\epsilon_0\epsilon_r}{q}\left(\frac{1}{N_a} + \frac{1}{N_d}\right)(V_{bi} + V_a)}. \tag{2.2}$$

Although the general physics in the formation of the pn-junction is similar to a SBC, many phenomena and applicational differences exist which include the image force, minority carrier injection, switching speed and so on. The depletion region can be expressed as

2.2 Point defects and charge carrier emission

Impurities and defects are important in order to provide a semiconductor with desirable electrical properties but may also be hightly unwanted and detrimental to the device performance, as shown in the previous section with the dopants. This section will discuss properties of defects and their roles with charge carriers.

2.2.1 Formation and stability of defects

In bulk materials, impurities and defects are introduced during growth and/or in the later processing steps. This can occur unintentionally by contamination from the environment or intentionally by various routes, such as ion-implantation and in-diffusion.

[1] $\epsilon_0 \simeq 8.854 \times 10^{-14}\, F/cm$
[2] $k = 1.381 \times 10^{-23} J/K$

Among the many lattice positions where a defect can be situated, Fig.2.2 shows a) an interstitial configuration and b) the substitutional configuration of a single impurity atom in a unit cell of silicon. Other defect configurations can, for instance, be bond-center, anti-bonding and hexagonal (32). More complicated configurations exist when

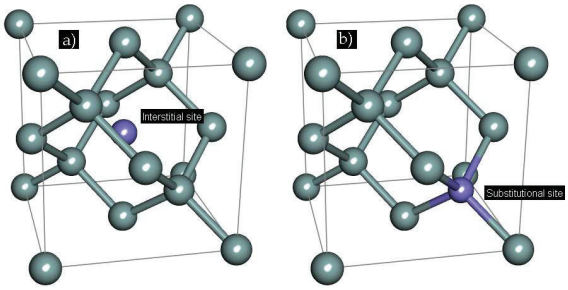

Figure 2.2: Unit cells of silicon crystal with a) a tetrahedral interstitial and b) a substitutional defect. The drawing is made using Accelrys DS Vizualizer 3.1.(33)

combining multiple defects. This generates the possibility of higher dimensional defect, such as the one-dimension (1D) line defect, plane defect (2D) and clusters (3D) (34).

The stability of a defect configuration is determined upon the energy barrier required to interchange between defect configurations (35). The probability of surmounting an energy barrier increases exponentially with increasing temperature. For that reason, heat treatments (annealings) is commonly performed to investigate the evolution of and the interactions between defects present in a crystal. Furthermore, a heat treatment is terminated by cooling the crystal back to room temperature (RT) with a certain cooling rate. When a crystal is slowly cooled, a defect finds the most stable configuration. However, when the crystal is rapidly cooled (quenched), defects can be frozen into configurations differing from the most stable one. Quenching is, therefore, widely used in the study of Fe in silicon to freeze the in-diffused Fe to the interstitial lattice position which may otherwise form other Fe-related defect complexes at room temperature. (7).

A defect can also change its stability by altering the energy barrier for interchanging to other configurations. This can be performed by a change in the charge state of a defect(36). When a defect is introduced in the crystal, it can generate one or more energy levels within the band gap, which defines the charge state transitions. Thus, moving the Fermi-level will result in filling or emptying a defect for charge carriers,

changing its charge state and, hence, its stability. As indicated in Sec.2.1 about SBC, the Fermi-level can easily be moved within the depletion region by applying a bias voltage in reverse. This enables a method of annealing in reverse bias voltage on a diode. The technique, not only allows a change in the defect annealing temperature, it also allows for defect reactions which would otherwise be hindered due to repulsion of same charge state (Coloumb repulsion).

2.2.2 Electron and hole occupancy of a defect

As electrically active defects and impurities form energy levels within the band gap, charge carriers can interact with the defects via the energy levels which results in filling or emptying of a defect of electrons and holes. Figure 2.3 shows the four possible charge carrier transitions between the energy bands and a defect, which changes the concentration of hole-filled (p_T) and electron-filled (n_T) defect from the total defect concentration ($N_T = p_T + n_T$). When a charge carrier is captured from and re-emitted

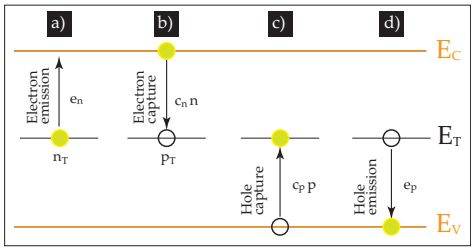

Figure 2.3: Schematics of capture and emission of charge carriers by a deep level, showing a) emission of an electron, b) capture of an electron, c) capture of a hole and d) emission of a hole.

to the same band, the transition is called trapping. While, if a charge carrier re-emits to the other band, it is called recombination. Such transitions are associated with the rates of capture and emission of holes ($c_p p$ and e_p, respectively) and electrons ($c_n n$ and e_n, respectively), where the capture rates are dependent on the concentration of electrons in the conduction band (n) and holes in the valence band (p). For a given n and p, electron occupancy of a defect can be deduced from the following partial

differential equation

$$\frac{dn_T}{dt} = c_n n p_T + e_p p_T - c_p p n_T - e_n n_T = (c_n n + e_p)(N_T - n_T) - (c_p p + e_n) n_T \,. \quad (2.3)$$

The equation can be solved for $n_T(t)$ to be

$$n_T(t) = n_T(0) e^{-t/\tau} + \frac{e_p + c_p n}{e_n + c_n n + e_p + c_p p} N_T (1 - e^{-t/\tau}) \,, \quad (2.4)$$

where $n_T(0)$ is the electron occupancy of the defect at $t = 0$ and $\tau = 1/(e_n + c_n n + e_p + c_p p)$. Similar equation for holes can be achieved by changing electron-related terms into hole-related terms.

Equation 2.4 can be reduced significantly when considering a defect in the depletion region which is initially filled with electrons ($n_T = N_T$) and in the process of being emptied. In such consideration, no free charge carriers are found in the bands ($n = p = 0$) and the electron emission is dominating ($e_n \gg e_p$), which results in an important equation for various characterization techniques, such as deep level transient spectroscopy,

$$n_T(t) \simeq n_T(0) e^{-t/\tau} = N_T e^{-e_n t}. \quad (2.5)$$

2.2.3 Capture and emission rate

The capture rate of electrons for a defect is defined as (37)

$$c_n n = v_{th,n} \sigma_n n \,, \quad (2.6)$$

where σ_n is the capture cross-section of the defect and $v_{th,n}$ is the average thermal velocity of the electrons. The thermal velocity is defined as $v_{th,n} = \sqrt{3kT/m_n^*}$, where m_n^* is the effective mass of electron[1]. Similar equation can be deduced for holes by exchanging the electron-related indexes with p.

The emission rate of electrons can be deduced by considering the principle of detailed balance, which states that (Ref.(37) p.307) "under equilibrium conditions each fundamental process and its inverse must balance independent of any other process that

[1] $m_n^* = 1.08 m_n$

may be occurring inside the material" . This means that electron capture and emission by a defect with the conduction band has to balance each other at equilibrium, leading to

$$e_{n0} n_T = c_{n0} n_0 (N_T - n_T), \tag{2.7}$$

where the index 0 denotes equilibrium. Inserting for N_T and n_T using the Fermi-Dirac distribution, the equilibrium emission rate becomes

$$e_{n0} = c_{n0} N_C \frac{g_0}{g_1} exp\left(-\frac{E_C - E_T}{kT}\right), \tag{2.8}$$

where g_0 is the degeneracy of an unoccupied state, g_1 is the degeneracy of an occupied state and N_C is the effective density of states in the conduction band. Under the assumption that the emission and the capture rates change insignificantly under non-equilibrium conditions, the 0-index for e_{n0} and c_{n0} can be removed. Non-equilibrium conditions can, for instance, involve contributions from electric field, which can affect the emission rate.

2.2.4 Poole-Frenkel effect

The Poole-Frenkel effect is one of the effects which alter the energy barrier for emission of charge carriers by an electrical field (38), for instance in a depletion region. This effect exists only if an emitted charge carrier experiences a Coloumb attraction to the same defect. Figure 2.4 shows schematically an energy potential of a defect where the energy barrier is reduced by an applied electrical field. The reduction in the energy

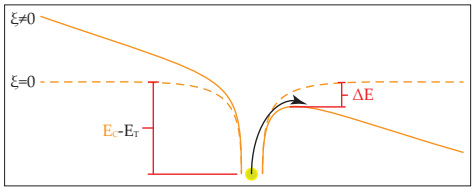

Figure 2.4: Schematic of Poole-Frenkel effect, showing energy barrier lowering for an electron emission from a defect due to an electrial field.

barrier can, in a one-dimensional approximation, be expressed as

$$\Delta E = 2q\sqrt{\frac{\xi q}{\epsilon_0 \epsilon_r}}, \tag{2.9}$$

where ξ is the absolute value of the electrical field.

The Poole-Frenkel effect can be utilized to identify acceptors in p-type material or donors in n-type material by observing a dependence of emission properties as a function of electrical field. However, the lack of Poole-Frenkel in p-type (n-type) material does not necessarily prove the nature of donor (acceptor) (39).

Chapter 3

Methods

In this chapter, three of the most essential electrical characterization techniques and a simulation tool used in the thesis will be described. The Capacitance-voltage (CV) measurement is mainly used in determining the charge carrier concentration as a function of depth in order to control the doping concentration of a wafer and to investigate changes in samples after treatments. Both deep level transient spectroscopy (DLTS) and admittance spectroscopy (ADSPEC) are used to investigate defects including their energy level position and concentrations.

3.1 Capacitance-voltage measurement (CV)

One of the most important quantities in characterizing a diode is the capacitance, and defined as (40)

$$C = \frac{\Delta q}{\Delta V}, \tag{3.1}$$

where Δq is the change in the charge and ΔV is the change in the voltage. Normally, the capacitance is extracted by use of an AC voltage signal (for instance 1 MHz) with a small probing amplitude (typically between 30 to 100 mV) and measuring the current response. In a capacitance-voltage measurement, the AC-signal is superpositioned with a stepwise-changing DC-signal. For an ideal diode, the capacitance follows a voltage-

dependence given as

$$C = A\sqrt{\frac{q\epsilon_0\epsilon_r}{2}\left(\frac{1}{N_a}+\frac{1}{N_d}\right)^{-1}\frac{1}{V_{bi}+V_a}}\,, \tag{3.2}$$

where A is the area of the junction. This equation can be simplified by introducing the depletion width (Eq.2.2) to

$$C = \frac{\epsilon_0\epsilon_r A}{W}\,, \tag{3.3}$$

which is an important equation in providing the depth-information under investigation.

From a capacitance-voltage measurement, information about the effective charge carrier concentration as a function of depth can be extracted by, for instance, the following relation (40)

$$N(W) = -\frac{2}{q\epsilon_0\epsilon_r A^2}\left(\frac{\Delta C^{-2}}{\Delta V_a}\right)^{-1}. \tag{3.4}$$

As an example, Fig.3.1 shows charge carrier concentration versus depth profiles for SBC before and after a heat treatment. It is known that formation of a SBC can unintentionally introduce hydrogen to the surface of the semiconductor (from, for instance, the metal), and that hydrogen passivates boron acceptors (32, 41, 42), forming the B-H complex, which reduces the charge carrier concentration. Thus, the amount of reduction in the charge carrier concentration can indirectly give information about the concentration of hydrogen. From Fig.3.1, it can also be seen that heat treatment can dissociate the B-H complex and distribute the hydrogen further into the semiconductor.

Equation 3.4 assumes a negligible or uniform concentration of deep-level defects. However, for a non-uniform concentration of deep acceptors (in n-type) in a sufficient amount to influence the overal carrier concentration, an artificial peak can occur (43).

3.2 Deep level transient spectroscopy (DLTS)

Deep level transient spectroscopy is a powerful electrical characterization technique capable of determining the majority capture cross-section, energy level position, concentration and depth profile of defects(44). This technique utilizes the transient response

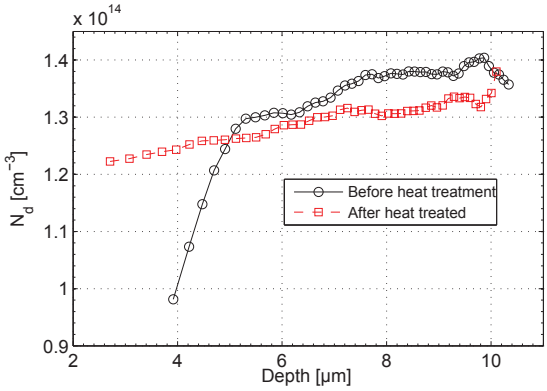

Figure 3.1: Charge carrier concentration versus depth profile before and after heat treatment on a aluminium SBC. It reveals the passivated region, which results from the formation of B-H, and can be related to the concentration of hydrogen.

of either capacitance, current or voltage due to emission of charge carriers from a defect level at different temperatures. Each charge carrier emission is initialized after a filling procedure of the defect. The principle of DLTS will be presented in the case of a p-type semicondutor and for capacitance transients.

Figure 3.2a shows schematically a SBC under reverse bias voltage with a depletion width of W_0. Two energy levels are drawn above and below the midgap in the p-

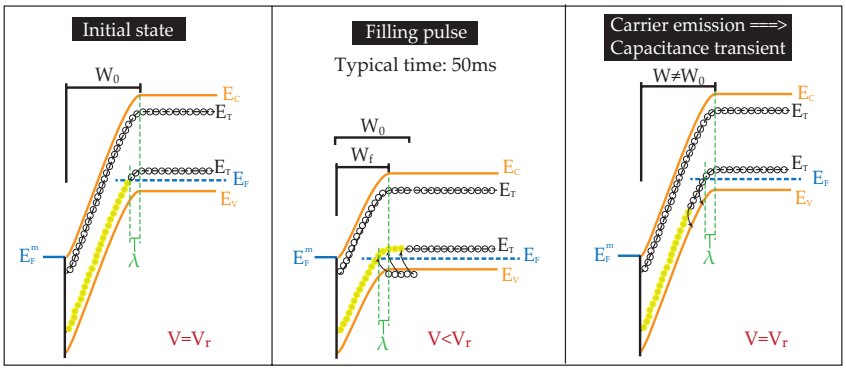

Figure 3.2: Schematics showing the principle of DLTS through filling and emptying of a defect in a SBC by a voltage pulse.

type semiconductor. The occupancy of the deep levels can be reasoned by considering the emission and capture rates of charge carriers described in Sec.2.2.2. For the deep level close to the E_C, the emission rate of electrons dominates over the emission rate of holes and the capture rate of electrons. Thus, this deep level remains emptied of electrons (filled with holes). For the deep level close to the E_V, the emission rate of holes dominates over the emission rate of electrons, but the emission rate of holes competes with the capture rate of holes which varies spatially. At the depth $W_0 - \lambda$, where λ is the distance from the edge of the depletion region to the crossing depth between the deep level and the Fermi-level, a transition in the dominance of capture and emission rate of hole occurs. Thus, it is convenient to adress the position of the Fermi-level relative to defect levels to discuss the occupancy of defect levels.

In Fig.3.2b, the reverse bias voltage of the SBC is removed. As a consequence, the depletion width is shorter than in Fig.3.2a and the Fermi-level moves below the region depleted of holes of the deep level between $(W_0 - \lambda)$ and $(W_f - \lambda)$. This leads to a capture process of holes, filling the defects.

When returning the SBC to its initial reverse bias voltage, shown in Fig.3.2c, the instantaneous depletion width differs from W_0 due to the change in occupancy of the defects within the depletion region. However, the defects in the region between $(W_0 - \lambda)$ and $(W_f - \lambda)$ are again under the Fermi-level which favours the emission of holes to the valence band. The process of emisson of holes creates a capacitive change as a function of time, yielding a capacitance transient, as simulated in Fig.3.3a for different temperatures. When $N_T \ll N_a$, the capacitance transient can be expressed as

$$\Delta C(t) = \frac{C_r N_T}{2N_a} e^{-e_p t}\,, \tag{3.5}$$

where C_r is the capacitance under reverse bias voltage immediately before the voltage pulse. From fitting of the measured capacitance transients to this equation, defect properties, like defect concentration, energy level position and capture cross-section, can be extracted. However, a more practical and visual method is available which involves weigthing functions.

3.2.1 Weighting functions

A typical DLTS measurement is performed by repeatedly acquiring the capacitance transient after a filling pulse while heating or cooling of the sample. The capacitance transients are averaged within a temperature interval and the raw data of a DLTS measurement may appear, for example, as simulated in Fig.3.3a. Such data representation are diffucult to work with, especially in comparing between different DLTS measurements. Thus, mathematical treatments are used in order to convert the data into a

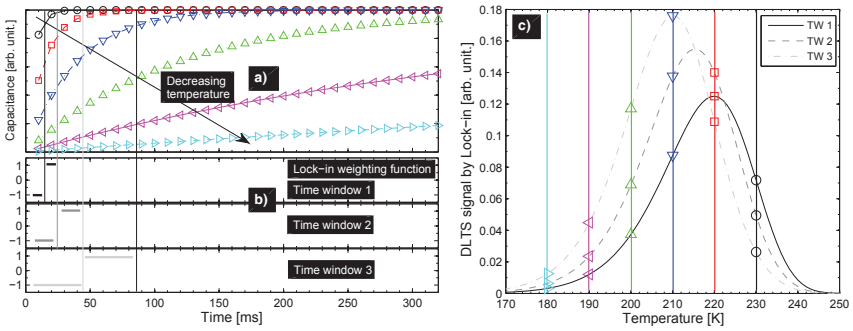

Figure 3.3: Principle of DLTS, simulated by Matlab, showing a) capacitance transients at different temperature, b) lock-in weighting function for the first three time-windows and c) DLTS spectra of the transients in *a)*, extracted using lock-in weighting function in *b)*.

spectrum with peaks as a function of temperature. Many weigthing functions exist which differ by their capability of seperating close-lying peaks and their tolerance of noise (45), for instance lock-in and GS4 weighting function, where a lock-in weighting function is widely used.

The lock-in weighting function provides a simple mathematical conversion with high tolerance of noise which is ideal for characterizing defects that are significantly different in charge carrier emission properties. This function converts the transient by simply subtracting the first half of the transient with the second half. Thus, the lock-in weighting function can be expressed as

$$w_{Lock-in}(t_j) = \begin{cases} -1 & \text{, for } 1 \leq j \leq 2^{i-1} \\ 1 & \text{, for } 2^{i-1} < j \leq 2^i \end{cases} \tag{3.6}$$

where t_j is a discretized time (10 ms in Fig.3.3a) and i is the time-window (TW) which represents the length of time to be considered. Figure 3.3b shows the lock-in weighting function for the first three time-windows which involves the first 2, 4 and 8 data points of the transients. This leads to time-window dependent DLTS signals, S_i, which are expressed as

$$S_i = \frac{1}{2^i} \sum_{j=1}^{2^i} w_{lock-in}(t_j) \Delta C(t_j) \,. \tag{3.7}$$

Figure 3.3c shows three DLTS spectra deduced from the transients in Fig.3.3a according to Eq.3.7 for the first three time-windows. A peak from each DLTS spectrum is visible due to a deep level and the peak position is shifted depending on the time-window. This shift is essential when extracting defect parameters.

In contrast to the lock-in weighting function, the GS4 weighting function has a lower tolerance to noise but higher capability (energy resolution) of seperating peaks. The function which is given as (46)

$$w_{GS4}(t_j) = \begin{cases} -1 & \text{, for } 1 \leq j \leq 2^{i-2} \\ 25 & \text{, for } 2^{i-2} < j \leq 2^{i-1} \\ -48 & \text{, for } 2^{i-1} < j \leq 3/2 \times 2^{i-1} \\ 24 & \text{, for } 3/2 \times 2^{i-1} < j \leq 2^i \end{cases} , \tag{3.8}$$

requires four data points of a transient for the first time-window ($i = 2$), and the DLTS signals are calculated with Eq.3.7 after replacing $w_{lock-in}$ with w_{GS4}. A detailed description of this weighting function can also be found in Ref.(47).

3.2.2 Extraction of defect parameters

Weighting functions have enabled the visualization of deep levels as peaks at given temperature depending on the parameters chosen for the time-windows. In addition, the temperature of a peak maximum represents an emission rate of a deep level at that temperature. Thus, using several time windows, a collection of emission rates at different temperatures are found. By rearranging Eq.2.8, a relation between the

emission rate and temperature can be expressed as

$$ln\left(\frac{e_n}{T^2}\right) = ln\left(\left[\frac{8\pi^{3/2}m_n^* k^2}{h^3}\right]\frac{g_0}{g_1}\sigma_n\right) - \left(\frac{E_C - E_T}{k}\right)\frac{1}{T}\,, \tag{3.9}$$

and visualized in an Arrhenius plot of $ln(e_n/T^2)$ versus $1/T$. Here, the slope of the Arrhenius plot uncovers the energy level position, while the extrapolated intersection to the ordinate gives the apparent capture cross-section. However, the above interpretations assume negligible change in the entropy when a charge carrier is emitted, which is explained more thoroughly in Appendix A.

The concentration of a deep level can be extracted by acquiring the ΔC at $t = 0$ and using Eq.3.5. This concentration represents an average value over the investigated depth which is, in many cases, appropiate for uniformly distributed defects (44). However, in the case of a non-uniform defect distribution, a depth profile over the region of interest is necessary to quantify the defect concentration.

3.2.3 Deep level depth profiling

DLTS can reveal the depth distribution of a deep level. Various measurement procedures allow to acquire the necessary information for extracting the depth profile of a deep level. However, the essence remains in varying the filling pulse in order to fill and empty deep levels at defined depths.

One method involves gradually changing the filling pulse from a fixed reverse bias voltage at a fixed temperature. Thus, for every increment of the amplitude of the filling pulse, the investigated depth expands and gives the depth information needed. With this method, the deep level concentration can be expressed as (40)

$$N_T(W_f - \lambda) = -\frac{qW_0^2}{\epsilon_0\epsilon_r}\left(\frac{W_f}{W_f - \lambda}\right)N_a^+(W_d)N_a^+(W_f)\frac{\delta(\Delta C_f/C_0)}{\delta V_f}\,, \tag{3.10}$$

where the conventions of the symbols are those in Fig.3.2. More specifically, C_0 is the capacitance at the fixed reverse bias voltage, C_f is the capacitance at the filling pulse voltage and

$$\lambda = \sqrt{\frac{2\epsilon_0\epsilon_r}{qN_a}(E_F - E_T)} \tag{3.11}$$

which is similar to Eq.2.2 on the depletion width.

As an example, from Paper III, Fig.3.4 shows the depth profiling of the FeB pair and the Fe_i before and after reverse bias annealing (RBA). This information is useful

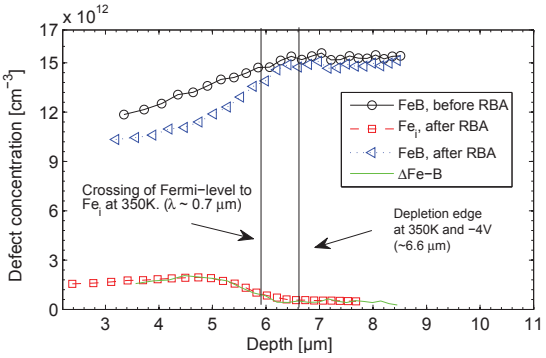

Figure 3.4: Defect concentration versus depth profiles for Fe-B and Fe_i measured before and after RBA.

in determining the region where the FeB pair has dissociated to form Fe_i. The measurements were acquired at 52 and 224K for the FeB pair and the Fe_i, respectively, and the fixed reverse bias voltage was 8V.

3.3 Admittance spectroscopy (ADSPEC)

Admittance spectroscopy has the similar capability as DLTS in the sense that this is also an electrical characterization technique to extract information about the energy level position, capture cross-section and concentration of defects (and dopants). The difference between ADSPEC and DLTS lies in the detection limits. While DLTS has better detection limit of the defect concentration than ADSPEC, ADSPEC has the capability of investigating shallow levels, including dopants.

Admittance spectroscopy can be performed by measuring the capacitance and/or conductance as a function of temperature in a diode structure (40, 48, 49). Since these quantities are measured by use of a small AC signal with a certain frequency, energy levels are affected by the constantly changing Fermi-level which results in an alternatively filling and emptying process of the energy levels by charge carriers. At

high temperatures, the emission of charge carriers is fast and the occupation of the energy levels respond to the AC frequency nearly instantaneously. On the other hand, at low temperatures, the emission rate of the charge carriers is low and they do not respond to the AC frequency. As a consequence, the capacitance will be reduced, while the conductance increases and reaches a peak value. Figure 3.5 shows ADSPEC data, where two peaks in the conductance spectra can be observed for each probing frequency. Each peak represent an energy level, which can be extracted using an Arrhenius plot

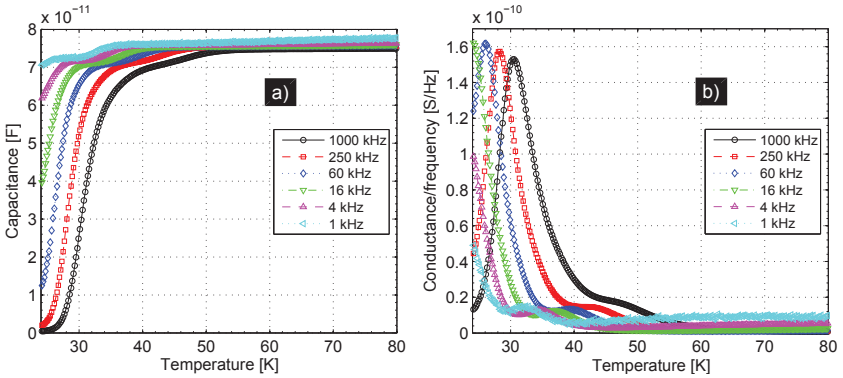

Figure 3.5: Admittance spectroscopy measurement, showing the a) the capacitance and b) the conductance versus the temperature. Two energy levels are present in the measurement.

with the following relation of

$$ln\left(\frac{2\pi f}{T^2}\right) \propto \frac{1}{T}\frac{E_T - E_V}{k}, \tag{3.12}$$

where f is the probing frequency and T is the absolute temperature where the peak occurs.

The capacitance in an ADSPEC signal can be expressed as(50)

$$\Delta C = \frac{\epsilon_0 \epsilon_r}{W}\frac{N_T}{N_D}\frac{1-\frac{W-\lambda}{W}}{1+\frac{W-\lambda}{W}\frac{N_T}{N_D}}, \tag{3.13}$$

where N_D is the doping concentration. From the Eq.3.13, it can be seen that the amplitude is significantly reduced when $(W-\lambda) \simeq W$. This condition occurs when the

energy level of defects is close to that of the dopants.

3.4 Simulation software (Synopsys TCAD)

Synopsys TCAD is a package of simulation softwares which can be used to simulate electrical properties of devices, such as diodes and transistors (51). When a structure is created using a Sentaurus Structure Editor (SentaurusSE), various electrical quantities can be solved using Sentaurus Device (SentaurusD), such as capacitance and conductance. This is performed by achieving a self-consistent solution between the Poisson's equation and the continuity equations for electrons and holes, respectively, expressed as:

$$\nabla\epsilon\nabla\phi = -q(p - n + N_d - N_a) - \rho \tag{3.14}$$

and

$$\nabla \cdot \vec{J_n} = qR_{net} + q\frac{\delta n}{\delta t} \qquad -\nabla \cdot \vec{J_p} = qR_{net} + q\frac{\delta p}{\delta t}, \tag{3.15}$$

where ϕ is the electrical potential, ρ is the concentration of traps and fixed charges (dopants excluded), $\vec{J_{n,(p)}}$ is the electron (hole) current density, R_{net} is the recombination rate and t is the time. From these equations, the electrical field and the flow of charge carrier can be described for a diode junction (Sec.2.1).

SentarausD allows for simulation with an applied AC signal for the purpose of calculating capacitance and conductance. When such a calculation is performed on a diode structure at different temperature, ADSPEC spectrum can easily be simulated. Furthermore, transient signals are also possible to acquire. With the proper simulation of trap conditions, a DLTS spectrum can be simulated whether it is a standard DLTS measurement, depth profiling, optical DLTS, capture cross-section measurement or other. Examples of command files for simulating ADSPEC and standard DLTS can be found in Appendix B.

Figure 3.6 shows a program which has the purpose of organizing the many different programs in the Synopsys software package. The left part lists all the available projects where a project "ADSPEC_ALSi_FrontImp_5e15_60Hz.tmp" is opened and shown in the right part. Two simulations tools (SentaurusSE and SentaurusD) are loaded and 30 simulations are performed with the temperature being the variable. This project is for

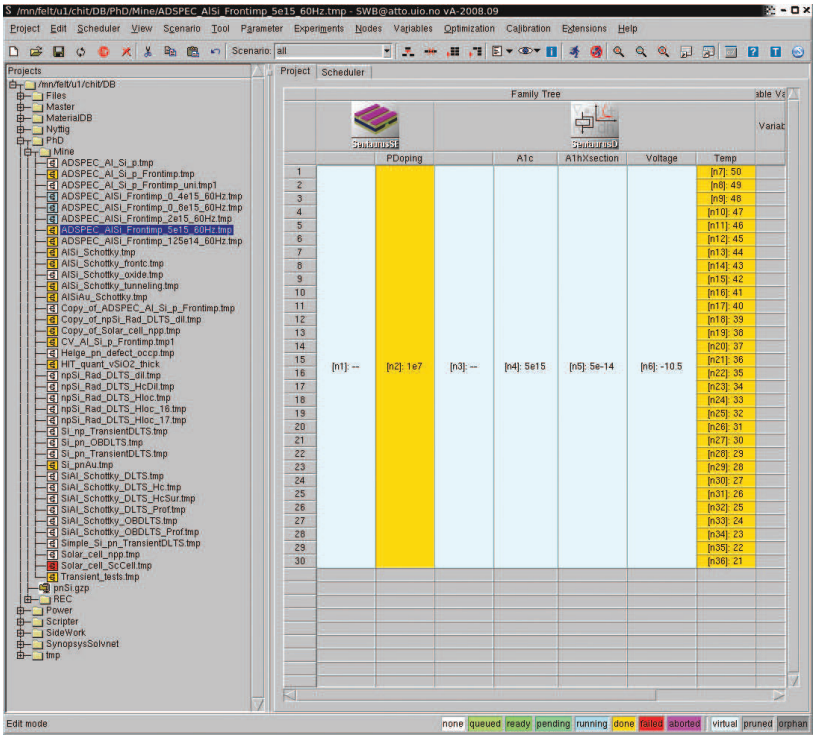

Figure 3.6: A graphical user interface program (Sentaurus Workbench) which allows for easy control over the different programs in the Synopsys software package.

an ADSPEC simulation in the temperature range between 21 to 50K (steps of 1) with a reverse bias voltage between 0 to -10.5 (with 20 steps, not visible in the Fig.3.6). One acceptor defect of interest is implemented with energy level position, concentration and hole capture cross-section of E_V+0.057 eV (not visible in Fig.3.6), $5\times10^{15}\,\mathrm{cm}^{-3}$ and $5\times10^{-14}\,\mathrm{cm}^{2}$, respectively.

Chapter 4

Present work and suggestions for future work

This chapter gives an insight into the work reported in this thesis. The main results of each paper are hightlighted and suggestions for future work are presented.

4.1 Material

The work in this thesis targets applications for solar cells with the main focus on Fe in silicon. Although multicrystalline silicon is the material which contains considerable amount of Fe, most of the studies are conducted using single crystalline silicon grown by Czochralski or float-zone method.

The single crystalline material is chosen in order to avoid contribution from other unintended impurities and defects that are common in multi-cyrstalline material. In addition to Fe impurities, the grain boundaries in multicrystalline silicon host many metal impurities such as copper, nickel and titanium (2). After high temperature treatments, these metals can dissolve into the grains, undergo various reactions and cause electrical signatures which can interfere with the signatures of Fe-related defects. This complicates the interpretation of data and provides a less reliable picture of the underlying reactions and mechanisms than in a material containing mainly Fe impurity. In as-grown single crystal silicon, the concentration of electrically active defects is

typically below the detection limit of DLTS, and, thus, provides a suitable model system for investigating reactions of intentionally introduced defects and impurities, such as Fe.

Furthermore, the non-uniformity of multicrystalline silicon can give rise to impurity distribution that varies laterally. Since DLTS, which can offer a high detection limit of four orders of magnitude below the doping concentration, does not enable easy mapping of a sample, spatial uniformity is preferable.

4.2 Preparation

With the underlining topic of Fe defects in silicon, a reliable and reproducible method to introduce a controllable amount of Fe is necessary. At the begining, following the literature (27), an easy method for introduction of Fe was tested where $FeCl_3$ was dissolved and applied to the samples. Thereafter, the samples were heat treated in a sealed vacuumed quartz ampoule to avoid cross contamination. However, DLTS measurements of the samples did not show any resemblence of previously reported results. In addition, no reversible reaction from the detected defects, which could indicate the presence of Fe, were observed. The reasons may possibly be the purity of the chemical, the cleanliness of the ampoule and/or the preparation environment, since the samples had to be transfered out of the clean room for sealing of the ampoule.

The latter method was therefore abandoned at an early stage and replaced by ion-implantation. This method provides reproducible and controlled introduction of Fe in silicon and with negligable contamination from other elements. In addition, it also allows for placement of Fe in different depths of the samples which is crucial in Paper VI.

To minimize cross contaminations during heat treatments while distributing Fe uniformly in the sample, a dedicated tube furnace was mainly used. The quartz tube was cleaned thoroughly by immersing the whole tube, along with any quartz boats and quartz tools, into a chemical solution (aqua regia, 3:1, HCl:HNO_3) overnight. Then, the tube and the tools were rinsed in de-ionized water for several minutes. The cleaniness of the tube furnace was usually tested before heat treating the experiment samples by exposing cleaned as-received samples under the same experimental conditions. Thereafter, these control samples were measured with DLTS to check for electrically active

defects introduced from the furnace. In some cases, the DLTS measurement on the control samples detected Fe_i in a concentration on the order of $10^{10}cm^{-3}$. This concentration was a factor of around 10^{-4} of the doping concentration and considered as acceptable.

4.3 Detected defects in this work

This section provides an overview of the electrically active defects discussed in the appended papers, with the purpose of easing the literature search for reader, and they are listed in Table 4.1. The apparent capture cross-sections are mainly extracted from

Table 4.1: Electrically active defects detected in the papers.

Label	E_V+XX [eV]	Apparent capture cross-section [cm^2]	Reference
Fe-B	0.10	4×10^{-15}	Paper II-V, (7)
Fe_i	0.40	3×10^{-16}	Paper II-V, (7)
H(0.3)	0.27 ±0.03	5×10^{-15}	Paper I
H(0.4)	0.38 ±0.03	1×10^{-15}	Paper I
H(0.17)	0.17	4×10^{-16}	Paper IV
H(0.28)	0.28	6×10^{-15}	Paper IV
H(0.34)	0.34	4×10^{-14}	Paper IV
H(0.25)	0.24	1×10^{-14}	Paper V
H(0.29)	0.29	9×10^{-15}	Paper V
H(0.34)	0.34	2×10^{-14}	Paper V
V_2	0.18	1×10^{-16}	Paper IV, V, (52, 53, 54)
C_i	0.30	3×10^{-14}	Paper V, (55)
C_iO_i	0.35	2×10^{-15}	Paper IV, V, (53, 55)
VOH	0.25	3×10^{-15}	Paper IV, (53, 56)
B_iC_s	0.29	2×10^{-14}	Paper V, (57)
V_2O	0.22	1×10^{-15}	Paper V, (58, 59)
Not labelled	0.06 (fitted: 0.057)	5×10^{-14} (fitted)	Paper VI

extrapolation of the Arrhenius plots which can give an uncertainty of 1-2 orders of magnitude. In addition, Arrhenius plot of the defect levels discussed in Paper IV and V are shown in Fig.4.1.

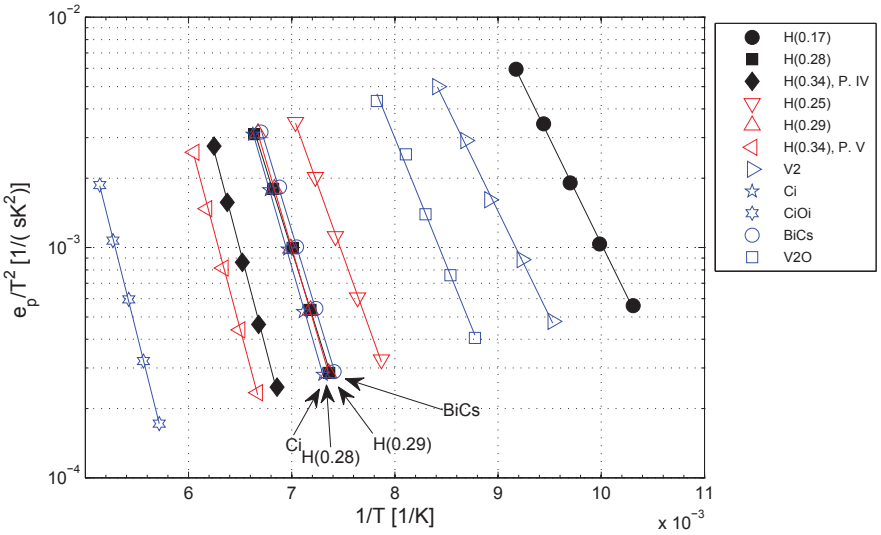

Figure 4.1: Arrhenius plots of the defect levels observed in Paper IV and V with corresponding defect properties shown in Table 4.1.

4.4 Paper I: Rapid thermal annealing-induced defects

In collaboration with the solar group at the Institutt for Energy Technology (IFE), multicrystalline silicon samples were rapid thermally annealed at 1000°C for 2 min. When the samples were investigated using DLTS, two significant electrically active deep levels were observed. The experiment was repeated using the same furnace with single crystalline wafers which had a lower doping concentration than the multicrystalline ones. By lowering the doping concentration, the detection limit for DLTS increases proportionally. In addition, the change in doping concentration might change the defect concentration which would suggest a defect involving the dopant (boron, in this case).

The two defects found in the multicrystalline sample appeared in the single crystalline ones as well, and various treatments and measurements were conducted to gather more information about their properties. It is found that the defects exhibit acceptor-like nature, are stable above 650°C and are most likely indiffused from the environment with high diffusivity. Comparing with the theoretical results, it is suggested that the

deep levels arise from two defects involving Fe and vacancies/boron.

In a later stage, the same experiment was conducted on n-type samples to investigate the upper part of the midgap. However, difficulties were experienced in producing a reliable Schottky barrier contact with gold on heat treated samples where the gold contacts could easily be wiped off even with a clean room wiper. It was suspected that the surface could be the reason for the problem, but they remained even when the samples were etched by several microns.

A future work could be to try to investigate these defects using DLTS with optical excitation on p-type samples. This can be performed with illumination at the rearside with light above the band gap energy.

4.5 Paper II & III: Interaction between H and Fe

Hydrogen interaction with Fe has been a topic of great interest in solar cells, since hydrogen is easily introduced during the processing steps and because hydrogen has a reputation of passivating defects, such as dangling bonds and vacancies (17, 60). From the literature, it has been suggested that hydrogen passivates Fe (25). However, it is also suggested that hydrogen dissociates the Fe-B pair (27, 61), forming Fe_i which is a detrimental defect in solar cells. Furthermore, theory predicts a reaction of hydrogen with Fe_i^0 (neutral), but not with Fe_i^+ (positively charged), and that the resulting Fe-H pair has energy levels in the band gap (28). This led to the interest of a further investigation, where concentration versus depth profiles were carefully considered for both the Fe-B pair, Fe_i and hydrogen, since both the Fe_i^+ and Fe_i^0 exists within a depletion region of a diode.

Thus, hydrogen was incorporated into Fe-contaminated boron-doped silicon samples and driven to regions of Fe_i with different charge states. The hydrogen incorporation was attempted on the samples through boiling in water (62), heated HF (63) and wet chemical etching (WCE) (with $HF:HNO_3:CH_3COOH$) (27, 64). The latter method was observed to be the most efficient one in terms of the amount of hydrogen introduced, as deduced from CV-measurements. However, the etching process occasionally produced rough surfaces and these samples were discarded.

After the etching, the samples were further cleaned and were Al deposited for SBC and stored for 1-2 weeks before commencing the measurements to allow the Fe_i,

which were dissociated from Fe-B during the etching, to reassociate with B. Thereafter, a continiuous process of measurements and treatments were performed for the CV-measurements, DLTS spectra, reverse bias annealing (RBA) and depth profiles. During the RBA, the temperature and the capacitance were constantly monitored.

The main results are shown in Fig.4.2 which shows the defect concentration versus depth profiles of the Fe-B pair and Fe_i for the WCE and non-WCE samples, both before and after RBA. Firstly, it can be noticed that the Fe-B pair dissociates due to the RBA

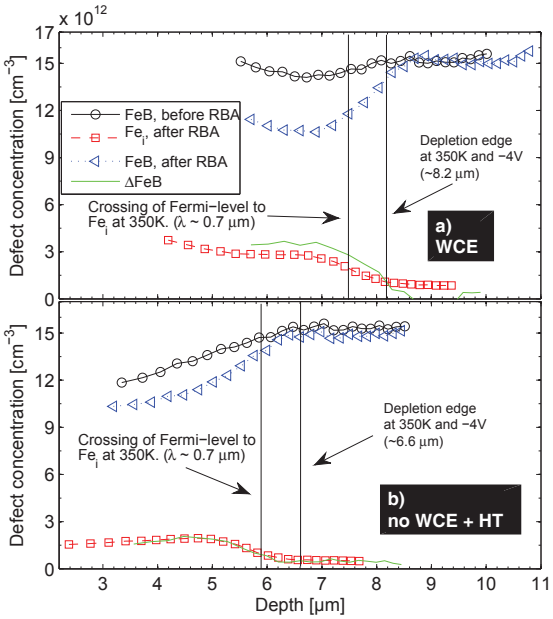

Figure 4.2: Defect concentration vs depth profile for Fe-B and Fe_i measured on (a)samples with WCE and (b)HT samples without WCE.

treatment and that the amount of released Fe_i is larger for WCE samples than the ones without WCE. Secondly, the concentration of Fe_i is significant only for the WCE samples in the region within the added vertical lines, which marks the depletion region containing Fe_i^+. This increase can not be explained by a diffusion of Fe_i due to the similarity in the reduction and increase in defect concentrations, nor can it be explained by a dissociation of the Fe-B pair due to the lack of Coulombic attraction between Fe

and B. Hence, the observations strongly point towards a reaction between hydrogen and the Fe-B pair which results in formation of B-H, releasing Fe_i^+. Furthermore, from the DLTS spectra after RBA, which shows no new signals and from the depth profiles, it is concluded that passivation of Fe by H has not been observed.

For future work, although no formation of Fe-H complexes is observed electrically in this work with reactants as Fe-B or Fe_i, it may be interesting to investigate interaction between hydrogen and other complexes of Fe. In the work by Wünstel and Wagner (65), several electrically active Fe-related defects were observed by different cooling rates. Although unidentified, electrical neutralizaion by hydrogen of these defects can be of technological interest, for instance, in solar cells.

4.6 Paper IV & V: Irradiation-induced defects and Fe

A recent theoretical study made an extensive investigation into defect reactions between Fe and irradiation-induced defects in silicon (66). The calculations predicted several stable electrically active defects which were not firmly established or observed. This opened up for experimental investigations with the ambition that the results could be utilized in the optimization of gettering of Fe.

The sample preparation involved irradiation of an Fe-contaminated sample and, thereafter, performing DLTS measurements. The Fe-contaminated samples were shipped to Sweden for electron irradiation at 6 MeV. However, a failure in the accelerator arised and the irradiation was put on hold. Several months of waiting turned into about one year, and the final message was that the accelerator will never be put up to meet the specified parameters again. Fortunately, the electron irradiation was eventually performed when Vladimir Markevich travelled to Minsk, but the energy had to be reduced to 4 MeV. The samples were then measured with DLTS and defects were investigated after different isochronal annealings for 30 min.

However, as one may have noticed, the study involving irradiation-induced defects with Fe was first reported on proton-irradiated samples from this Ph.D. work and not electron-irradiated samples. While waiting for electron irradiation, proton irradiation was performed with the ion-implanter at MiNa-lab. The energy of the protons was set to the highest capability such that the projected range would be located a factor of 2-3 deeper than the region probed using DLTS. This was to minimize the contribution

of hydrogen on the investigated defects. Still, indications that hydrogen had been incorporated in the probing region was observed through the detection of a defect with the characteristics of the vacancy-oxygen-hydrogen (VOH) in the reference samples. This introduction of hydrogen, however, could also have occured during the preparation of the samples, for instance from the deposited metal contact.

A number of different defects have been detected through the experiments with electron or proton irradiation on Fe-contaminated and boron-doped samples, as shown in Figs.4.3 and 4.4. These defect levels are labelled according to their energy level position, where H(0.17) has an energy level position at E_V+0.17 eV. The investigation

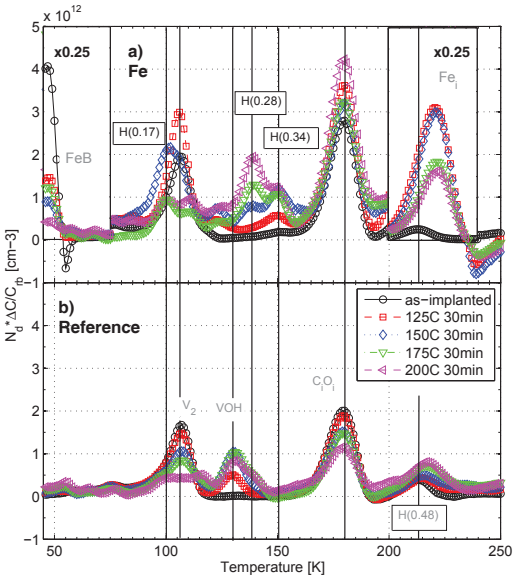

Figure 4.3: Spectra of DLTS measurements, with GS4 weighting function, on proton-irradiated Fe-contaminated and reference samples after different subsequent annealing temperature for 30 min. It shows three distinctive peaks (H(0.17), H(0.28) and H(0.34)) which are only found in the Fe-contaminated samples. These spectra are extracted from rate-window of $(320\,\mathrm{ms})^{-1}$.

of the defects through isochronal annealing has aided in the understanding of the relation between the different defects. In proton-irradiated samples, the concentration

of H(0.34) is observed to follow the concentration of VOH in the reference samples. In addition, no signal indicating VOH in the Fe-contaminated samples is found. This indicates that H(0.34) and VOH are related either by a common precursor or that the VOH is a precursor for H(0.34) and, thus, indicating a reaction between Fe and VO.

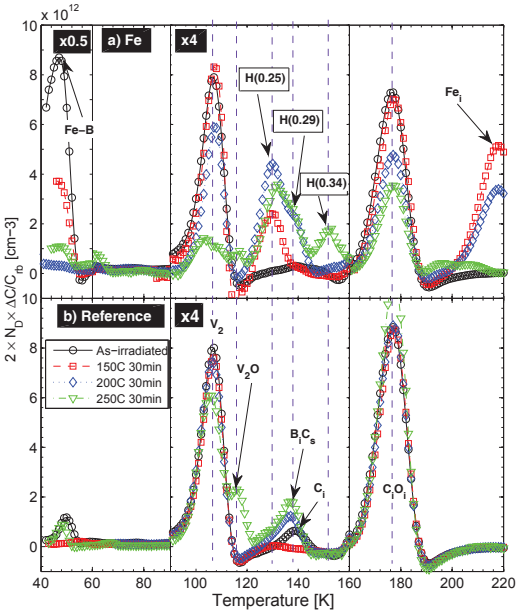

Figure 4.4: Spectra of DLTS measurements, with GS4 weighting function, on electron-irradiated Fe-contaminated and reference samples at as-implanted state and annealed at 150, 200 and 250K for 30 min. It shows three distinctive peaks (H(0.25), H(0.29) and H(0.34)) which are only found in the Fe-contaminated samples. These spectra are extracted from rate-window of $(640\text{ms})^{-1}$

Furthermore, the proton-irradiated Fe-contaminated samples contain a defect (H(0.28)) which evolves in its concentration towards the as-irradiated concentration of V_2, suggesting a relation between Fe and V_2. The same suggestion is made when Fe-contaminated samples are investigated after electron-irradiation. In these samples, the concentration of H(0.29) is observed to increase according to the loss of V_2 for annealing temperatures below 225°C when assuming that the DLTS signal of H(0.29) is overlapping with B_iC_s. For annealing at 225 and 250°C, this relation deviates significantly, however, a

peak (H(0.34)) is observed to emerge at those temperatures which compensate for the difference reasonably well. From these observations, it is further suggested that H(0.34) is another configuration of a complex between Fe and V_2.

Future work would be to repeat the experiments with epitaxially grown silicon that has a low content of oxygen and carbon. In addition, annealing at higher temperature should also be performed to investigate for further formation of Fe-related defects. Hydrogenation of electron-irradiated samples can be performed to investigate the H(0.34) defect in the proton-irradiated samples.

4.7 Paper VI: Fe-assisted formation of a shallow acceptor

Further motivated by the calculations performed in Ref.(66), a search for the substitutional Fe was initiated. The configuration, $^0Fe^0$ (neutral and no spin), is predicted to be highly stable with a gain in energy of 2.92 eV when compared with isolated $^1Fe_i^0$ and the monovacancy, $^0V^0$. This shows that Fe can react with the monovacancy and that this reaction can potentially be utilized for gettering and/or removal of the harmful effect of Fe_i. However, the existence of substitutional Fe is only evidenced by Mössbauer spectroscopy(67) and β^- emission channeling measurements(68).

Based on the similar method of preparation of samples as in Ref.(68), p-type silicon was implanted with Fe and heat treated at different temperatures. Thereafter, the samples were characterized electrically using CV, DLTS and ADSPEC. The temperatures for heat treatment were first investigated at 400°C with the idea that the majority of the prominent irradiation-induced defects would be annealed out. However, charge carrier concentration versus depth profiles, deduced from CV measurements, showed compensation at the projected range and towards the surface which was too large to extract reliable data from DLTS. Still, DLTS and optical DLTS measurements were performed with the aim to detect distinctive differences between the Fe-implanted and Si-implanted samples. However, no significant difference could be drawn for that annealing temperature and up to 650°C. After annealing at 800°C, a full recovery of the doping profiling was achieved for the reference samples (silicon-implanted). It was then clear that an enhancement of the acceptor concentration at the projected range exists only in the Fe-implanted samples and not in the Si-implanted samples.

This peak was further investigated on samples with different implantation doses of Fe and Si, spanning from 5 to 625% of the doping concentration at the calculated implantation peak. Still, the peaks are only found in the Fe-implanted samples, and it is observed that the enhancement in the acceptor concentration has a close to one-to-one relation with the implanted dose. Different ADSPEC measurements were performed on the samples to reveal the electrical properties of the defect. Figure 4.5 shows the ADSPEC measurements on the samples with different implantation doses of Fe and the corresponding fitted curves from Sentaurus TCAD. The inset shows an enlarged

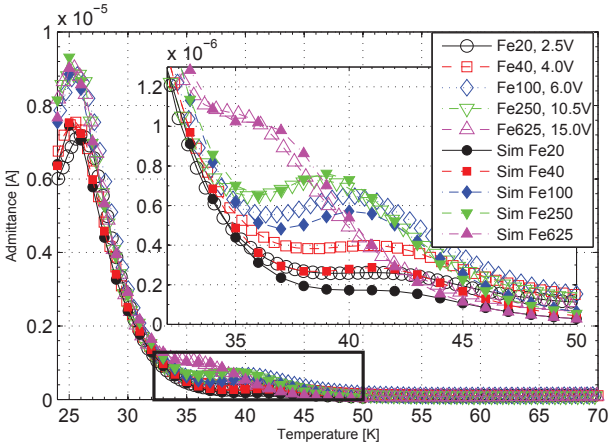

Figure 4.5: Admittance spectroscopy on Fe20, Fe40, Fe100, Fe250 and Fe650 samples, showing an increase in the amplitude of a peak with increasing Fe implantation dose. In addition, simulated curves using Sentaurus TCAD are shown for the corresponding experimental curves.

picture of the marked area, where a signal can be observed to increase with increasing dose of the Fe implantation. Furthermore, a shift in the peak position towards low temperature occurs for increasing dose. The latter observation shows that the defect obeys the Poole-Frenkel effect and, thus, acts as an acceptor. This shows that the enhanced acceptor concentration observed with CV measurements is caused by this defect.

At that point, it was believed that the defect configuration could be substitutional Fe. However, chemical identification of the presence of Fe was necessary in order to

support the assignment. Thus, secondary ion-mass spectrometry (SIMS) was performed both using the SIMS in our lab and externally. Figure 4.6 shows the SIMS depth profiles of samples implanted with different doses of ^{54}Fe. Unexpectingly, SIMS measurements

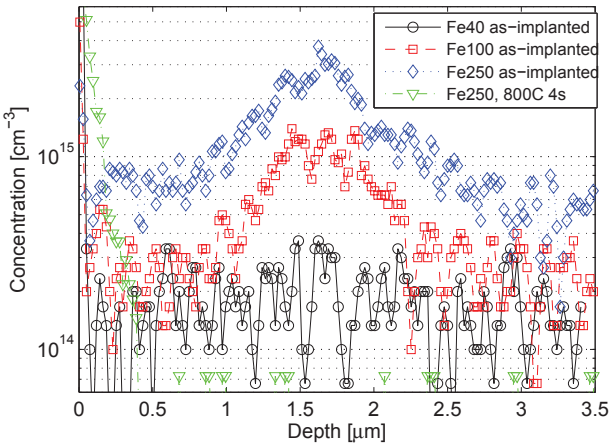

Figure 4.6: SIMS results for the on ^{54}Fe40, ^{54}Fe100 and ^{54}Fe250 samples, showing the concentration of ^{54}Fe as a function of depth for as-implanted and annealed samples..

show that Fe diffuses out of the projected range region during the heat treatment and that the final defect, thus, does not contain Fe. Hence, the presence of Fe only assists the formation of a shallow defect.

Suggestions for future works are extensive, due to the interesting and challenging behaviour observed for the first time. Firstly, experiments should be performed to investigate the chemical composition of the defect by, for instance, varying the concentration of dopant, oxygen and carbon. Furthermore, the type of dopant can also be varied. Secondly, the assisted formation of this shallow defect can be investigated through implantation of elements with similar chemical behaviour as Fe. Thirdly, diffusion and stability of this shallow acceptor can be investigated through isochronal and isothermal annealings.

Appendix A

Emission rate and capture cross-section

The emission rate of electron can be, deduced from Eq.2.8, written as

$$e_n = v_{th,n}\sigma_n N_C \frac{g_0}{g_1} exp\left(-\frac{E_C - E_T}{kT}\right). \tag{A.1}$$

This equation is often used to extract the E_T and the capture cross-section, σ, of defect levels in the band gap. The capture cross-section is commonly deduced through the intercept of the ordinate in a $ln(e_n/T^2)$ versus $1/T$ plot. However, this pratice can give errors by a factor of 10-100, as shall be discussed.

Thermodynamically, the emission of electron is a change in the Gibbs energy, ΔG, given as

$$\Delta G = E_C - E_T = \Delta H - T\Delta S, \tag{A.2}$$

where H is the entalphy and S is the entropy of the defect. Inserted in Eq.A.1, the emission rate of electron can be expressed as

$$e_n = v_{th,n}\sigma_n N_C \frac{g_0}{g_1} exp\left(\frac{\Delta S}{k}\right) exp\left(-\frac{\Delta H}{kT}\right). \tag{A.3}$$

Thus, comparing with Eq.A.1, the extraction of the capture cross-section from an Arrhenius plot has an additional factor of $exp(\Delta S/k)$, which can produce an error of a few orders of magnitude when assuming that ΔS is negligable (37).

One method to determine the capture cross-section more accurately is by an alternative method of DLTS. In contrast to the standard DLTS measurement, the voltage pulse duration is varied at a constant temperature at the occurance of a DLTS peak. With a short pulse duration, the filling of the defect level is close to 0, while with a long pulse width, the defect level becomes saturated. The transition can be fitted, for

capture of electrons, with (69)

$$n_T(t_p) = n_T(\infty)(1 - exp(-c_n n t_p)), \tag{A.4}$$

where t_p is the voltage pulse duration. It should be noted that the saturation time of the defect is exponentially dependent on the doping concentration. For silicon with doping concentration of 10^{16}cm^{-3} and a defect level with capture cross-section of 10^{-14}cm^2, the saturation time is in the order of 10 ns. This puts a high requirement on the performance of the instruments. To avoid this problem, the doping concentration of the material can be reduced to meet the capability of instruments.

Appendix B

Software command files

Command files for SentaurusSE and SentaurusD are shown for an example of ADSPEC and DLTS simulation.

B.1 ADSPEC simulation

In this simulation. the important output files which contains the information about the voltages, conductances and capacitances are the "ADSPEC_60e3_n<node>_ac_des.plt", where <node> is a number assigned for the different simulations. From Fig.3.6, the <node> is any real number between 7 to 38.

Variables need to be specified in Sentaurus Workbench are: $PDoping$ for the doping concentration, $A1c$ for a defect concentration, $A1hXsection$ for capture cross-section of the defect, $Voltage$ for the different simulation voltages (20 steps from 0V to $Voltage$) and $Temp$ for the temperature. These inputs are also shown in Fig.3.6.

Structure file (for SentaurusSE)

```
(sdegeo:set-default-boolean "ABA")

(define width 50)
(define height 25)
(define Pdoping @PDoping@)

;---------Structure-----------
(sdegeo:create-rectangle (position 0 0 0) (position width height 0)
   "Silicon" "region1")
(sdegeo:create-rectangle (position 0 0.8 0) (position width 2.2 0)
   "Silicon" "ProjRange")

;---------Doping--------------
(sdedr:define-constant-profile "Const.P1" "BoronActiveConcentration" Pdoping)
(sdedr:define-constant-profile-region "PlaceC.P1" "Const.P1" "region1")

(sdedr:define-constant-profile "Const.P2" "BoronActiveConcentration" Pdoping)
```

```
(sdedr:define-constant-profile-region "PlaceC.P2" "Const.P2" "ProjRange")

;---------Contact--------------
(sdegeo:define-contact-set "SchottkyC" 4 (color:rgb 0 0 1) "##")
(sdegeo:define-2d-contact (find-edge-id (position (/ width 2) 0 0)) "SchottkyC")

(sdegeo:define-contact-set "OhmicC" 4 (color:rgb 0 1 0) "##")
(sdegeo:define-2d-contact (find-edge-id (position (/ width 2) height 0)) "OhmicC")

(render:rebuild)

;--------Refinement------------
(sdedr:define-refinement-window "RefWinContact1" "Rectangle" (position 0 0 0)
   (position width 3 0) )
(sdedr:define-refinement-window "RefWinRest" "Rectangle" (position 0 0 0)
   (position width height 0))
#(sdedr:define-refinement-window "RefWinBoundary" "Rectangle" (position 0.75 0 0)
   (position 3 height 0) )

(sdedr:define-refinement-size "RefDefContact1" width  (/ 1 100) width (/ 1 150) )
(sdedr:define-refinement-placement "PlaceRFContact1" "RefDefContact1" "RefWinContact1")

(sdedr:define-refinement-size "RefDefRest" width  (/ 1 1) width (/ 1 25) )
(sdedr:define-refinement-placement "PlaceRFRest" "RefDefRest" "RefWinRest")

#(sdedr:define-multibox-size "MB.Channel" (/ 1 1) (/ 1 500) 100 100 1 1.35)
#(sdedr:define-multibox-placement "PlaceMB.Channel" "MB.Channel" "RefWinBoundary")

;-----------save and build--------------------
(sdeio:save-tdr-bnd (get-body-list) "@tdrboundary/o@")
(sdedr:write-cmd-file "@commands/o@")
(system:command "mesh -f tdr n@node@_msh")
```

Calculation file (for SentaurusD)

```
###################### Devive A ################################
Device AlSiSchottkyA {
   File {
      Grid = "@tdr@"
      Param = "@parameter@"
      Current = "@plot@"
      Plot    = "@tdrdat@"
   }

################ Define contact type ####################
   Electrode {
      {Name="SchottkyC" Voltage=0 Material="Aluminum" Schottky}
      {Name="OhmicC" Voltage=0 }
   }
############## End define contact type ####################
   Physics {
      Mobility (DopingDep HighFieldsat Enormal)
      EffectiveIntrinsicDensity( OldSlotboom )
      Temperature=@Temp@
   }

   Physics (Material = "Silicon") {
      Traps(
```

```
         (Acceptor Level EnergyMid=0.044 fromValBand
         Conc=2e15 hXsection=7e-14 eXsection=2000e-13
         Add2TotalDoping PooleFrenkel)
      )
   }

   Physics (Region = "ProjRange") {
      Traps(
         (Acceptor Level EnergyMid=0.057 fromValBand
         SpatialShape=Gaussian SpaceMid=(25 1.5 0) SpaceSig=(100 0.2 0)
 Conc=@A1c@ hXsection=@A1hXsection@ eXsection=1e-1
 Add2TotalDoping PooleFrenkel )

 (Acceptor Level EnergyMid=0.044 fromValBand
 Conc=2e15 hXsection=7e-14 eXsection=1e-20
 Add2TotalDoping PooleFrenkel)
      )
   }
}
################ End devive A ################################

File{
   Output  = "@log@"
   ACExtract = "@acplot@"
}

Plot {
   eDensity  hDensity  eCurrent  hCurrent
   eQuasiFermi hQuasiFermi  eVelocity  hVelocity
   eMobility  hMobility  eLifeTime hLifeTime
   eTrappedCharge hTrappedCharge
   eGapStatesRecombination  hGapStatesRecombination
   "hRelativeEffectiveMass" "eRelativeEffectiveMass"
   "hEffectiveStateDensity" "eEffectiveStateDensity"
   hGradQuasiFermi eGradQuasiFermie Eparallel hEparallel

   Potential  SpaceCharge  ElectricField
   Doping  DonorConcentration  AcceptorConcentration
   BandGapNarrowing EffectiveBandGap

   AugerRecombination SRHRecombination TotalRecombination
   Band2Band "BuiltinPotential" TotalTrapConcentration

   EffectiveBandGap EffectiveIntrinsicDensity
   ConductionBandEnergy ValenceBandEnergy
   Bandgap RefractiveIndex ElectronAffinit
   Temperature Band2Band EquilibriumPotential
}

Math {
   Extrapolate
   RelErrControl
   Digits=8
   Error=1e-10
   NotDamped=30
   Iterations=5

   ErrRef(Electron)=1.0e10
   ErrRef(Hole)=1.0e10
   ExtendedPrecision
}
```

```
System {
   AlSiSchottkyA diode1 (SchottkyC=s OhmicC=b)
   Vsource_pset  vs (s 0) {dc=0}
   Vsource_pset  vb (b 0) {dc=0}
}

Solve {
   Coupled (iterations=500){Poisson}
   Coupled (iterations=100) {Poisson hole}
   Coupled (iterations=100) {Poisson hole electron}

   NewCurrentPrefix="ADSPEC_60e3_"
   Quasistationary (
   InitialStep=1e-5 MaxStep=1 MinStep=1.e-20
   Goal { Parameter=vb.dc Voltage=@Voltage@ }
      ){ ACCoupled (StartFrequency=60e3 EndFrequency=60e3 NumberOfPoints=1
         Decade Node(b s) ACCompute (Time = (Range = (0 1)  Intervals = 20))
         ){Poisson hole electron}
   }

   System("rm ADSPEC*diode*.plt")
}
```

B.2 DLTS simulation

In this simulation. the important output files which contains the information about the capacitance in a transient are the "Cap<point>_n<node>_ac_des.plt", where <point> is a number for the different simulated point in a transient. Only two points from a capacitance transient are simulated in the program file for SentaurusD, which allows for simulating the first time-window of a lock-in weighting function. However, more transient points can easily be added and simulated with the cost of an increase in the computation time.

Three parameters are needed in the Sentaurus Workbench: *PDoping* for acceptor doping concentration, *Voltage* for the reverse bias voltage (the pulse voltage is 0 V) and *Temp* for the different temperatures.

Structure file (for SentaurusSE)

```
(sdegeo:set-default-boolean "ABA")

(define width 100)
(define height -500)
(define Pdoping @PDoping@)

;---------Structure------------
(sdegeo:create-rectangle (position 0 0 0) (position width height 0)
   "Silicon" "base")
(sdegeo:create-rectangle (position 0 (+ height 0.8) 0) (position width
```

```
   (+ height 1.3) 0) "Silicon" "defect")

;---------Doping---------------
(sdedr:define-constant-profile "Const.P1" "BoronActiveConcentration" Pdoping)
(sdedr:define-constant-profile-region "PlaceC.P1" "Const.P1" "base")
(sdedr:define-constant-profile-region "PlaceC.P2" "Const.P1" "defect")

;---------Contact--------------
(sdegeo:define-contact-set "BC" 4 (color:rgb 0 0 1) "##")
(sdegeo:define-2d-contact (find-edge-id (position (/ width 2) 0 0)) "BC")

(sdegeo:define-contact-set "FC" 4 (color:rgb 0 1 0) "##")
(sdegeo:define-2d-contact (find-edge-id (position (/ width 2) height 0)) "FC")

(render:rebuild)

;--------Refinement------------
(sdedr:define-refinement-window "RefWinJC" "Rectangle" (position 0 height 0)
   (position width (+ 3.0 height) 0) )
(sdedr:define-refinement-window "RefWinRest" "Rectangle" (position 0
   (+ height 3.5) 0) (position width 0 0) )

(sdedr:define-refinement-size "RefDefJC" (/ width 1) (/ 1 200) (/ width 1)
   (/ 1 250) )
(sdedr:define-refinement-placement "PlaceRFJC" "RefDefJC" "RefWinJC")

(sdedr:define-refinement-size "RefDefRest" (/ width 1)  (/ 1 1.1 ) (/ width 1)
   (/ 1 10) )
(sdedr:define-refinement-placement "PlaceRFRest" "RefDefRest" "RefWinRest")

;-----------save and build--------------------
(sdeio:save-tdr-bnd (get-body-list) "@tdrboundary/o@")
(sdedr:write-cmd-file "@commands/o@")
(system:command "mesh -f tdr n@node@_msh")
```

Calculation file (for SentaurusD)

```
Device AlSiSchottky {
   File {
      Grid = "@tdr@"
      Param = "@parameter@"
      Current = "@plot@"
      Plot    = "@tdrdat@"
   }

######################## Define contact type ##########################
   Electrode {
      {Name="FC" Voltage=0 Workfunction=4.0 Schottky}
      {Name="BC" Voltage=0}
   }
#################### End define contact type ########################

################### Physics ######################################
   Physics {
      Mobility (DopingDep HighFieldsat Enormal)
      EffectiveIntrinsicDensity( OldSlotboom )
      Temperature=@Temp@
   }
```

```
   Physics (Region = "defect") {
      Traps(
         (Donor Level EnergyMid=0.25 fromCondBand
         Conc=1e13 hXsection=1e-15 eXsection=1e-15
         ElectricField Add2TotalDoping )

         (Acceptor Level EnergyMid=0.4 fromValBand
         Conc=2e13 hXsection=1e-15 eXsection=1e-15
         ElectricField Add2TotalDoping )
      )
   }
}
################### End physics ####################################

File{
   Output  = "@log@"
   ACExtract = "@acplot@"
}

Plot {
   eDensity  hDensity  eCurrent  hCurrent
   eQuasiFermi hQuasiFermi  eVelocity  hVelocity
   eMobility  hMobility  eLifeTime hLifeTime
   eTrappedCharge hTrappedCharge
   eGapStatesRecombination  hGapStatesRecombination
   "hRelativeEffectiveMass" "eRelativeEffectiveMass"
   "hEffectiveStateDensity" "eEffectiveStateDensity"
   hGradQuasiFermi eGradQuasiFermi
   eEparallel hEparallel eDirectTunneling hDirectTunneling
   eBarrierTunneling hBarrierTunneling
   Potential  SpaceCharge  ElectricField
   Doping  DonorConcentration  AcceptorConcentration
   BandGapNarrowing EffectiveBandGap
   AugerRecombination SRHRecombination TotalRecombination
   Band2Band "BuiltinPotential" TotalTrapConcentration
   EffectiveBandGap EffectiveIntrinsicDensity
   ConductionBandEnergy ValenceBandEnergy
   Bandgap ElectronAffinity
   RefractiveIndex EquilibriumPotential
}

Math {
   #Extrapolate
   RelErrControl
   Rhsmin=1e-10
   Digits=8
   Error=1e-10
   NotDamped=100
   Iterations=80

   Method=ParDiSo #(NonsymmetricPermutation IterativeRefinement=15)
   Transient=BE
   Number_of_Threads=2
   WallClock

   ExtendedPrecision
}

System {
   AlSiSchottky diode1 (FC=b BC=s)
```

```
   Vsource_pset  vs (s 0) {dc=0}
   Vsource_pset  vb (b 0) {dc=0}
}

Solve {
   Poisson
   Coupled (Iterations=100){Poisson Electron}
   Coupled (Iterations=100){Poisson Hole}
   Coupled (Iterations=100){Poisson Electron}
   Coupled (Iterations=100 Method=Blocked LineSearchDamping=0.1
      NotDamped=3) {Poisson Electron Hole}

   set(TrapFilling=Frozen)
   Save(FilePrefix="InitSave00")
   #### Ramp to reverse bias ####
   Quasistationary (
   InitialStep=1e-1 MaxStep=1 MinStep=1.e-15
   Goal { Parameter=vs.dc Voltage=@Voltage@ }
   ){ACCoupled (StartFrequency=1e6 EndFrequency=1e6
          NumberOfPoints=1 Decade Iterations=10 Node(s b)
          ACCompute (Time = (Range = (0 1)  Intervals = 2))
             ){ Poisson Electron Hole }
   }
   Save(FilePrefix="InitSave0")

   #### Calculate the capacitance at @Voltage@ ####
   NewCurrentPrefix="CapInit_"
   Quasistationary (
   InitialStep=1e-1 MaxStep=1 MinStep=1.e-6
   Goal { Parameter=vs.dc Voltage=@Voltage@ }
   ){ACCoupled (StartFrequency=1e6 EndFrequency=1e6
          NumberOfPoints=1 Decade Node(s b)
          ACCompute (Time = (Range = (0 1)  Intervals = 2))
             ){ Poisson Electron Hole }
   }
   Save(FilePrefix="InitSave")

   #### Release the traps and start the transient sim. ####
   Unset(TrapFilling)
   Transient (
      InitialTime = 0 # [s]
      FinalTime = 0.015 # [s]
      # ----- Control the time step size -----
      InitialStep = 1e-4
      MinStep = 1e-15
      MaxStep = 5.e-1
      ) {Coupled(Iterations=10){ Poisson Electron Hole }
   }
   Set(TrapFilling=Frozen)
   Save(FilePrefix="Save1_")

   ############ Transient point 1 ###############

   NewCurrentPrefix="Cap1_"
   Quasistationary (
   InitialStep=1e-2 MaxStep=0.3 MinStep=1.e-6
   Goal { Parameter=vs.dc Voltage=@Voltage@ }
      ){ ACCoupled (StartFrequency=1e6 EndFrequency=1e6
```

```
      NumberOfPoints=1 Decade Node(s b)
      ACompute (Time = (Range = (0 1)  Intervals = 4))
         ){ Poisson Electron Hole }
      }

   Unset(TrapFilling)
   Transient (
      InitialTime = 0 # [s]
      FinalTime = 0.01 # [s]
      # ----- Control the time step size -----
      InitialStep = 1e-4
      MinStep = 1e-10
      MaxStep = 5.e-1
      ) {Coupled(Iterations=25){ Poisson Electron Hole }
   }
   Set(TrapFilling=Frozen)
   Save(FilePrefix="Save2_")

   ############ Transient point 2 ##############

   NewCurrentPrefix="Cap2_"
   Quasistationary (
   InitialStep=1e-2 MaxStep=0.3 MinStep=1.e-6
   Goal { Parameter=vs.dc Voltage=@Voltage@ }
   ){ACCoupled (StartFrequency=1e6 EndFrequency=1e6
     NumberOfPoints=1 Decade Node(s b)
     ACompute (Time = (Range = (0 1)  Intervals = 4))
        ){ Poisson Electron Hole }
     }

   System("rm Save_*")
   System("rm Cap?_diode1*")
}
```

References

[1] Please visit: http://www.pennenergy.com/index/power/display/5783356394/articles/Photovoltaics-World/industry-news/2011/2/solar-pv_s_zeitgeist.html. 1

[2] T. Buonassisi, A. A. Istratov, M. D. Pickett, M. Heuer, J. P. Kalejs, G. Hahn, M. A. Marcus, B. Lai, Z. Cai, S. M. Heald, T. F. Ciszek, R. F. Clark, D. W. Cunningham, A. M. Gabor, R. Jonczyk, S. Narayanan, E. Sauar, and E. R. Weber. **Chemical natures and distributions of metal impurities in multicrystalline silicon materials**. *Prog. Photovolt: Res. Appl.*, **14**:513–531, 2006. 1, 25

[3] G. Coletti, R. Kvande, V. D. Mihailetchi, L. J. Geerligs, L. Arnberg, and E. J. Øvrelid. **Effect of iron in silicon feedstock on p- and n-type multicrystalline silicon solar cells**. *J. Appl. Phys.*, **104**:104913, 2008. 1

[4] A. A. Istratov, T. Buonassisi, R. J. McDonald, A. R. Smith, R. Schindler, J. A. Rand, J. P. Kalejs, and E. R. Weber. **Metal content of multicrystalline silicon for solar cells and its impact on minority carrier diffusion length**. *J. Appl. Phys.*, **94**(10):6552, 2003. 1

[5] D. Macdonald, A. Cuevas, A. Kinomura, Y. Nakano, and L. J. Geerligs. **Transition-metal profiles in a multicrystalline silicon ingot**. *J. Appl. Phys.*, **97**:033523, 2005. 1

[6] C. B. Collins and R. O. Carlson. **Properties of silicon doped with iron or copper**. *Phys. Rev.*, **108**(6):1409, 1957. 1

[7] A. A. Istratov, H. Hielsmair, and E. R. Weber. **Iron and its complexes in silicon**. *Appl. Phys. A*, **69**:13–44, 1999. **and references therein**. 1, 8, 27

[8] A. A. Istratov, H. Hielsmair, and E. R. Weber. **Iron contamination in silicon technology**. *Appl. Phys. A*, **70**:489–534, 2000. **and references therein**. 1

[9] J. H. Reiss, R. R. King, and K. W. Mitchell. **Charaterization of diffusion length degradation in Czochralski silicon solar cells**. *Appl. Phys. Lett.*, **68**(23):3302, 2008. 1

[10] G. Zoth and W. Bergholz. **A fast, preparation-free method to detect iron in silicon**. *J. Appl. Phys.*, **67**(11):6764, 1990. 2

[11] A. Kaniava, A. L. P. Rotondaro, J. Vanhellemont, U. Menczigar, and E. Gaubas. **Recombination activity of iron-related complexes in silicon studied by temperature dependent carrier lifetime measurements**. *Appl. Phys. Lett.*, **67**(26):3930, 1995. 2

[12] A. L. P. Rotondaro, T. Q. Hurd, A. Kaniava, J. Vanhellemont, E. Simoen, M. M. Heyns, and C. Clays. **Impact of Fe and Cu contamination on the minority carrier lifetime of silicon substrates**. *J. Electrochem. Soc.*, **143**:3014, 1996. 2

[13] H. Hieslmair, A. A. Istratov, S. A. McHugo, C. Flink, T. Heiser, and E. R. Weber. **Gettering of iron by oxygen precipitates**. *Appl. Phys. Lett.*, **72**(12):1460, 1998. 2

[14] M. Horikawa and K. Terashima. **Comparison of iron gettering effectiveness in silicon between ion-implantation-induced damage and poly-crystalline silicon**. *Jpn. J. Appl. Phys.*, **41**:7267–7271, 2002. 2

[15] J. L. Benton, P. A. Stolk, D. J. Eaglesham, D. C. Jacobson, J.-Y. Cheng, J. M. Poate, N. T. Ha, T. E. Haynes, and S. M. Myers. **Iron gettering mechanisms in silicon**. *J. Appl. Phys.*, **80**(6):3275, 1996. 2

[16] M. Syre, S. Karazhanov, B. R. Olaisen, A. Holt, and B. G. Svensson. **Evaluation of possible mechanisms behind P gettering of iron**. *J. Appl. Phys.*, **110**:024912, 2011. 2

[17] E. V. Monakhov, A. Ulyashin, G. Alfieri, A. Yu. Kuznetsov, B. S. Avset, and B. G. Svensson. **Divacancy annealing in Si: Influence of hydrogen**. *Phys. Rev. B*, **69**:153202, 2004. 2, 29

[18] J. I. Pankove, M. A. Lampert, and M. L. Tarng. **Hydrogenation and dehydrogenation of amorphous and crystalline silicon**. *Appl. Phys. Lett.*, **32**(7):439, 1978. 2

[19] R. Lüdemann. **Hydrogen passivation of multicrystalline silicon solar cells**. *Mat. Sci. Eng. B*, **58**:86–90, 1999. 2

[20] S. Martinuzzi, I. Périchaud, and F. Warchol. **Hydrogen passivation of defects in multicrystalline silicon solar cells**. *Sol. Energ. Mat. Sol. C.*, **80**:343–353, 2003. 2

[21] J. I. Pankove, D. E. Carlson, J. E. Berkeyheiser, and R. O. Wance. **Neutralization of shallow acceptor levels in silicon by atomic hydrogen**. *Phys. Rev. Lett.*, **51**(24):2224, 1983. 2

[22] E. Ö. Sveinbjörnsson and Olof Engström. **Reaction kinetics of hydrogen-gold complexes in silicon**. *Phys. Rev. B*, **52**(7):4884, 1995. 2

[23] J.-U. Sachse, E. Ö. Sveinbjörnsson, W. Jost, and J. Weber. **Electrical properties of platinum-hydrogen complexes in silicon**. *Phys. Rev. B*, **55**(24):16176, 1997. 2

[24] N. Yarykin, J.-U. Sachse, J. Weber, and H. Lemke. **Electrically active silver-hydrogen complexes in silicon**. *Mater. Sci. Forum*, **258-263**:301–306, 1997. 2

[25] A. Azzizi, L. J. Geerligs, and D. Macdonald. **Hydrogen passivation of iron in crystalline silicon**. *Proc. 19th Europ. PVSEC, Paris*, pages 1021–1024, 2004. 2, 29

[26] M. Kouketsu and S. Isomae. **Hydrogen passivation of iron-related hole traps in silicon**. *J. Appl. Phys.*, **80**(3):1485–1487, 1996. 2

[27] OV Feklisova, AL Parakhonsky, EB Yakimov, and J Weber. **Dissociation of iron-related centers in Si stimulated by hydrogen**. *Mat. Sci. Eng. B*, **71**:268–271, 2000. 2, 26, 29

[28] M. Sanati, N. Gonzalez Szwacki, and S. K. Estreicher. **Intersitial Fe in Si and its interactions with hydrogen and shallow dopants**. *Phys. Rev. B*, **76**:125204, 2007. 2, 29

[29] N. Gonzalez Szwacki and S. K. Estreicher. **First-principles investigations of Fe-H interactions in silicon**. *Physica B*, **401-402**:171–174, 2007. 2

[30] Ben G. Streetman and Sanjay Kumar Banerjee. *Solid state electronic devices, 6th ed.* Pearson Prentice Hall, 2000. 5, 7

[31] L. H. Rhoderick and R. H. Williams. *Metal-Semiconductor contacts.* Clarendon Press, 1988. 5

[32] J. Chevallier and B. Pajot. **Interaction of hydrogen with impurities and defects in semiconductors**. *Solid State Phenom.*, **85-86**:203–284, 2002. 8, 14

[33] Please visit: http://accelrys.com/products/discovery-studio/visualization-download.php. 8

[34] Richard Tilley. *Understanding solids.* Wiley, 2006. 8

[35] Charles Kittel. *Introduction to solid state physics.* Wiley, 2005. 8

[36] L. C. Kimerling and J. L. Benton. **Electronically controlled reactions of interstitial iron in silicon**. *Physica B&C*, **116**:297–300, 1983. 8

[37] Dieter K. Schroder. *Semiconductor material and device characterization.* Wiley, 1990. 10, 37

[38] J. Frenkel. **On pre-breakdown phenomena in insulators and electronic semiconductors**. *Phys. Rev.*, **54**:647–648, 1938. 11

[39] W. R. Buchwald and N. M. Johnson. **Revised role for the Poole-Frenkel effect in deep-level characterization**. *J. Appl. Phys.*, **64**:958, 1988. 12

[40] P. Blood and J. W. Orton. *The electrical charaterization of semiconductors: Majority carriers and electron states.* Academic Press, 1992. 13, 14, 19, 20

[41] S. J. Pearton, J. W. Corbett, and M. Stavola. *Hydrogen in crystalline semiconductors.* Springer-Verlag, 1992. 14

[42] M. W. Horn, J. M. Heddleson, and S. J. Fonash. **Permeation of hydrogen into silicon during low-energy hydrogen ion beam bombardment**. *Appl. Phys. Lett.*, **51**:490, 1987. 14

[43] L. C. Kimerling. **Influence of deep traps on the measurement of free-carrier distributions in semiconductors by junction capacitance techniques**. *J. Appl. Phys.*, **45**(4):1839, 1974. 14

[44] D. V. Lang. **Deep level transient spectroscopy: A new method to characterize traps in semiconductors**. *J. Appl. Phys.*, **45**:3023, 1974. 14, 19

[45] A. A. Istratov. **Critical analysis of weighting functions for the deep level transient spectroscopy of semiconductors**. *Meas. Sci. Technol.*, **9**:477, 1998. 17

[46] A. A. Istratov. **New correlation procedure for the improvement of resolution of deep level transient spectroscopy of semiconductors**. *J. Appl. Phys.*, **82**(6):2965, 1997. 18

[47] Denny Åberg. *Capacitance spectroscopy of point defects in silicon and silicon carbide.* PhD thesis, Kungliga Tekniska Högskolan, 2001. 18

[48] D. L. Losee. **Admittance spectroscopy of impurity levels in Schottky barriers**. *J. Appl. Phys.*, **46**(5):2204, 1975. 20

[49] G. Vincent, D. Bois, and P. Pinard. **Conductance and capacitance studies in GaP Schottky barriers**. *J. Appl. Phys.*, **46**(12):5173, 1975. 20

[50] J. L. Pautrat, B. Katircioglu, N. Magnea, D. Bensahel, J. C Pfister, and L. Revoil. **Admittance spectroscopy: A powerful characterization technique for semiconductor crystals - Application to ZnTe**. *Solid State Electron*, **23**:1159–1169, 1980. 21

[51] Synopsys. **Sentaurus device manual**, 2007. 22

[52] B. G. Svensson, A. Hallén, J. H. Svensson, and J. W. Corbett. **Divacancy acceptor levels in ion-irradiated silicon**. *Phys. Rev. B*, **43**(3):2292, 1991. 27

[53] H. Malmbekk, L. Vines, E. V. Monakhov, and B. G. Svensson. **Hydrogen decoration of vacancy related complexes in hydrogen implanted silicon**. *Solid State Phenom.*, **178-179**:192–197, 2011. 27

[54] P. M. Mooney, L. J. Cheng, M. Süli, J. D. Gerson, and J. W. Corbett. **Defect energy levels in boron-doped silicon irradiated with 1-MeV electrons**. *Phys. Rev. B*, **15**:3836, 1977. 27

[55] J. Lalita, N. Keskitalo, A. Hallén, C. Jagadish, and B. G. Svensson. **Defect evolution in MeV ion-implanted silicon**. *Nucl. Instrum. Meth. B*, **120**:27–32, 1996. 27

[56] O. Feklisova, N. Yarykin, Eu. Yakimov, and J. Weber. **Hydrogen interaction with defects in electron-irradiated silicon**. *Physica B*, **273-274**:235–238, 1999. 27

[57] O. J. Drevinsky, C. E. Caefer, S. P. Tobin, J. C. Mikkelsen, JR., and L. C. Kimerling. **Influence of Oxygen and Boron on Defect Production in Irradiated Silicon**. In *MRS Proceedings 1987*, **104**, 1987. 27

[58] M. Mikelsen, E. V. Monakhov, G. Alfieri, B. S. Avset, J. Härkönen, and B. G. Svensson. **Annealing of defects in irradiated silicon detector materials with high oxygen content**. *J. Phys. Condens. Mat.*, **17**:S2247, 2005. 27

[59] M.-A. Trauwaert, J. Vanhellemont, H. E. Maes, A.-M Van Bavel, G. Langouche, and P. Clauws. **Low-temperature anneal of the divacancy in p-type silicon: A transformation from V_2 to V_xO_y complex?** *Appl. Phys. Lett.*, **66**(22):3065, 1995. 27

[60] N. Yarykin, O. V. Feklisova, and J. Weber. **Hydrogenation of the dominant interstitial defect in irradiated boron-doped silicon**. *Physical Review B*, **69**(045201), 2004. 29

[61] E. B. Yakimov and A. L. Parakhonsky. **Hydrogen stimulated destruction of Fe-B pairs in p-Si**. *Solid State Phenom.*, **57-8**:383–386, 1997. 29

[62] A. J. Tavendale, A. A. Williams, and S. J. Pearton. **Hydrogen injection and neutralization of boron acceptors in silicon boiled in water**. *Appl. Phys. Lett.*, **48**(9):590, 1986. 29

[63] J. J. Bleka, I. Pintilie, E. V. Monakhov, B. S. Avset, and B. G. Svensson. **Rapid annealing of the vacancy-oxygen center and the divacany center by diffusing hydrogen in silicon**. *Phys. Rev. B*, **77**:073206, 2008. 29

[64] T. Sadoh, K. Tsukamoto, A. Baba, D. Bai, A. Kenjo, T. Tsurushima, H. Mori, and H. Nakashima. **Deep level of iron-hydrogen complex in silicon**. *J. Appl. Phys.*, **82**(8):3828, 1997. 29

[65] K. Wünstel and P. Wagner. **Iron-related deep levels in silicon**. *Solid State Commun.*, **40**:797–799, 1981. 31

[66] S. K. Estreicher, M. Sanati, and N. Gonzalez Szwacki. **Iron in silicon : Interactions with radiation defects, carbon, and oxygen**. *Phys. Rev. B*, **77**:125214, 2008. 31, 34

[67] G. Weyer, A. Burchard, M. Fanciulli, V. N. Fedoseyev, H. P. Gunnlaugsson, V. I. Mishin, R. Sielemann, and the ISOLDE collaboration. **The electronic configuration of substitutional Fe in silicon**. *Physica B*, **273-274**:363–366, 1999. 34

[68] U. Wahl, J. G. Correia, E. Rita, J. P. Arajo, and J. C. Soares. **Lattice sites of implanted Fe in Si**. *Phys. Rev. B*, **72**:014115, 2005. 34

[69] Niclas Keskitalo. *Irradiation induced defects for lifetime control in silicon*. PhD thesis, Uppsala University, 1997. 38

I

II

III

Interaction between hydrogen and the Fe-B pair in boron-doped p-type silicon

C. K. Tang,[a] L. Vines, B. G. Svensson, and E. V. Monakhov
University of Oslo, Physics department/Center for Materials science and Nanotechnology, P.O. Box 1048 Blindern, Oslo N-0316, Norway

(Received 16 May 2011; accepted 12 July 2011; published online 4 August 2011)

The effect of hydrogen incorporation into iron-contaminated boron-doped Cz-Si has been investigated using deep level transient spectroscopy. In-diffusion of hydrogen by wet chemical etching followed by reverse bias annealing of Al, Schottky diodes result in the appearance of the defect level characteristic to interstitial iron (Fe_i), and the concentration of iron-boron pairs (Fe-B) decreases correspondingly. Quantitative observations from various defect concentration versus depth profiles imply strongly that H promotes dissociation of Fe-B releasing Fe_i whereas no detectable passivation of Fe-B or Fe_i by H occurs. © *2011 American Institute of Physics*. [doi:10.1063/1.3619848]

Iron in silicon is well known for its effect in degrading the performance of devices, such as in integrated circuits and solar cells.[1] Significant reduction in minority carrier lifetime, even at low iron concentration, is one of the main issues in solar cells based on p-type multicrystalline silicon. The efficiency of lifetime recovery by reducing the concentration of electrically active iron-related defects through gettering or passivation has frequently been investigated.[2–5] For the passivation, especially hydrogen has been studied. However, experimental reports on the effects of hydrogen on the iron behavior have shown various results. On one hand, passivation of iron by hydrogen was concluded through lifetime measurement.[4] On the other hand, deep level transient spectroscopy (DLTS) studies have observed an increase in the lifetime killing interstitial Fe (Fe_i) as possibly due to stimulated dissociation of the Fe-B pair by hydrogen.[6,7] In the latter reports, wet chemical etching (WCE) was performed to introduce H at the surface which resulted in an increase of Fe_i in the region where B-H was formed. Annealing under reverse bias led to an increase in the Fe_i signal in the depletion region and an indication of a small peak at the depletion edge where B-H reached its maximum concentration. Two mechanisms for release of Fe_i were discussed in Refs. 6 and 7. The first one involves a change in the Fermi-level position and changing the charge state of Fe_i from positive to neutral, which reduces the binding energy between Fe and B^- and quenches the formation of Fe-B.[8] The second one involves hydrogen in a reaction with Fe-B forming Fe_i and B-H but no decrease in Fe-B equivalent to the increase of Fe_i as a function of depth has been verified yet.

The interaction between Fe_i, Fe-B, and H has recently been predicted through *ab-initio* calculations using Vienna Ab-initio Simulation Package (VASP) and Spanish Initiative for Electronic Simulations with Thousands of Atoms (SIESTA) by Sanati *et al.*[9] The stability of various *a priori* configurations was estimated in different charge and spin states. In the case of Fe-B and H, it was predicted that the most stable configuration consists of an isolated $^{3/2}Fe_i^+$ and $^0B\text{-}H^0$ with 3/2 and 0 spin state, respectively. The gain in energy was 0.25 eV compared to $^{3/2}Fe\text{-}B^0$ and $^0H_{BC}^+$ (H in bond centered configuration). In addition, a stable configuration was also predicted between Fe_i and H, in the case of $^1Fe_i^0$. The gain in energy varied with the H reactant in $^{1/2}H_{BC}^0$ and $^0H_{BC}^+$ states to be 0.82 and 0.40 eV, respectively. The resulting Fe-H pair exhibits a deep donor level at 0.36 eV (SIESTA: 0.42 eV) above the valence band edge (E_V) and a deep acceptor level at 0.26 eV (SIESTA: 0.30 eV) below the conduction band (E_C). However, an additional H could release the Fe from Fe-H by forming Fe_i and H_2.

The charge state of Fe_i can easily be modified in a diode structure by applying an external bias which moves the Fermi-level and interchange Fe_i^+ to Fe_i^0. Such an experiment provides the opportunity for examining possible reaction between Fe_i^0 with H^+ which should appear in a specific region and give rise to new energy level positions, as predicted theoretically.

In this study, we have incorporated hydrogen in iron-contaminated p-type silicon through wet chemical etching and investigated its effects on iron. The results of different defect concentration versus depth profiles strongly favour dissociation of Fe-B in the presence of H, where the absolute loss in the concentration of Fe-B is accompanied by a corresponding gain in the concentration of Fe_i. In addition, our results show no detectable passivation of Fe_i and Fe-B by H.

Samples were cut from as-grown Czochralski Si wafers of p-type with a boron doping concentration of $\sim 1.3 \times 10^{14}$ cm^{-3}. Iron was introduced by ion implantation on the backside of the samples with energy and dose of 700 keV and 7×10^{11} cm^{-2}, respectively. Heat treatment was thereafter performed at 900 °C under nitrogen flow for 1 h in a tube furnace to distribute the Fe homogeneously in the samples. After the heat treatment, the samples were quenched rapidly in water to room temperature (RT).

WCE was performed for 30 s (7:5:2, HNO_3:HF:CH_3COOH) on one set of samples in order to introduce hydrogen at the surface.[7] Reference samples, which did not undergo WCE, were dipped in HF. All samples were, thereafter, further cleaned in RCA3 (H_2O, HCl, H_2O_2, 5:1:1, at 80 °C). Schottky barrier (SB) contacts were realized by thermal evaporation of Al through a metal mask on the front-surface

[a]Electronic mail: c.k.tang@smn.uio.no.

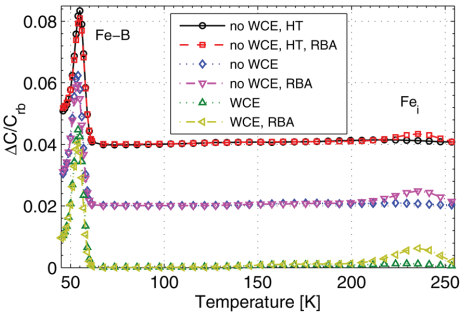

FIG. 1. (Color online) DLTS spectra before and after RBA on iron-contaminated samples with/without WCE treatment. The curves are taken with a rate window of (40 ms)$^{-1}$. An offset in $\Delta C/C_{rb}$ has been applied to the data for samples without WCE for clarity.

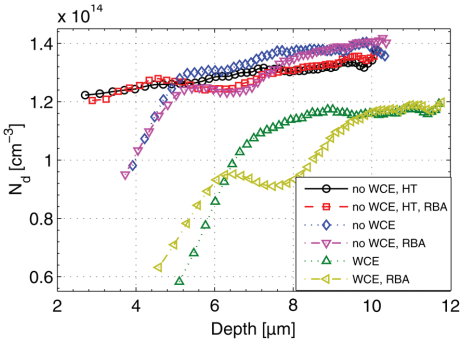

FIG. 2. (Color online) Charge carrier concentration vs depth profile before and after RBA on samples with/without WCE treatment. It reveals the passivated region, which results from the formation of B-H, and can be related to the concentration of hydrogen.

and Ohmic contacts were achieved by applying silver-paste on the back-side. Since the sample processing steps may introduce unintentional hydrogen at the surface, one set of the reference samples were heat treated (HT) at 180 °C for 30 min to distribute any accumulated hydrogen into the sample. Reverse bias annealing (RBA) was performed at 350 K for 30 min with a reverse bias voltage (V_{rb}) of 4 V.

DLTS measurements were performed with a V_{rb} of 8 V, pulse bias of −8 V, and pulse width of 50 ms in the temperature range of 40 to 300 K. The DLTS signal was extracted using a lock-in weighting function, and six rate-windows ranging from (5 ms)$^{-1}$ to (160 ms)$^{-1}$. The first DLTS measurements were performed after two weeks of storage at room temperature after the sample preparation.

Figure 1 shows DLTS spectra before and after RBA on samples with and without WCE treatment. Before RBA, one dominant peak can be observed at 55 K in all samples, with a defect concentration of 1.2×10^{13} cm^{-3}. From the result from the different rate windows, the energy level position and apparent capture cross-section were deduced to be $E_V + 0.10$ eV and 4×10^{-15} cm^2, respectively. The obtained values are in good agreement with the identification of the peak as Fe-B.[1] After RBA, a second peak appeared at 242 K with energy level position at $E_V + 0.40$ eV and apparent capture cross-section 3×10^{-16} cm^2, in good agreement with previous identification of Fe$_i$.[1] During storage at RT, the Fe$_i$ peak decreased in all samples while the Fe-B peak increased correspondingly. The evolution of the peaks is due to the (re)association of Fe$_i$ with B forming the Fe-B pair. This behaviour is a well known characteristic of Fe in boron-doped silicon, where the stable Fe-B pair can dissociate in a reversible reaction into Fe$_i$ by thermal treatment, illumination or minority carrier injection.[10] Although all samples experienced the RBA, the samples treated in WCE showed a higher DLTS signal of Fe$_i$ than the samples without WCE. In particular, it can be noticed that the HT sample exhibits a weak Fe$_i$ signal. However, from the Fig. 1, it can be misleading to conclude on a direct interaction between hydrogen and Fe, since changes in the charge carrier concentration (from RBA) can affect the DLTS signal.

Figure 2 shows the charge carrier concentration versus depth measured by capacitance-voltage measurement for the corresponding samples in Fig. 1. The charge carrier concentration can be related to the hydrogen concentration due to the formation of the B-H pair which is electrically inactive.[11] Accordingly, Fig. 2 unveils a considerable concentration of hydrogen in the near-surface region in the reference and the WCE-treated samples, while no change in carrier concentration is observed in the HT samples. Interestingly, a small concentration of hydrogen in the WCE samples has penetrated beyond 12 μm, seen as a reduced carrier concentration in the WCE samples compared to samples without WCE. The effect is also observed in other methods for hydrogen incorporation[12] and shows a large migration length of H despite efficient trapping by B. After RBA, a larger degree of passivation of B by H can be observed, causing a carrier concentration minimum, except for the HT sample which remains only slightly affected. The minimum in carrier concentration occurs at the depletion edge and is due to the electric field in the depletion region forcing/drifting the H^+ to the depletion edge, resulting in an accumulation of hydrogen.[13] It should also be mentioned that the debonding process of B-H has been reported to occur at a much higher rate within the depletion region compared to the quasi-neutral region.[14]

Figure 3 shows the concentrations of FeB and Fe$_i$ versus depth profiles for WCE samples and HT samples. The appearance of Fe$_i$ and the correlated loss in Fe-B, observed in Fig. 1, originates from a distinct layer, defined by RBA, within the DLTS depletion region.

As mentioned previously, one possibility for the release of Fe$_i$ is a change in the charge state of Fe$_i$ from positive to neutral which has been shown, by Kimerling and Benton,[8] to extinguish the pairing of Fe$_i$ and B^-. Since the applied reverse bias during RBA raises the Fermi-level above the level of Fe$_i$ (transferring it to the neutral state), the resulting defect profiles may be caused by the Fermi-level effect within the depletion region. It should be emphasized that the region where Fe changes the charge state is not located at the depletion edge but a distance closer to the surface, due to the so-called lambda-length.[15] Thus, release of Fe$_i$ should not occur at the depletion edge.

The depletion edge and the significance of the lambda-length are highlighted in Fig. 3 with added lines. The depth of the depletion region is determined from the capacitance that

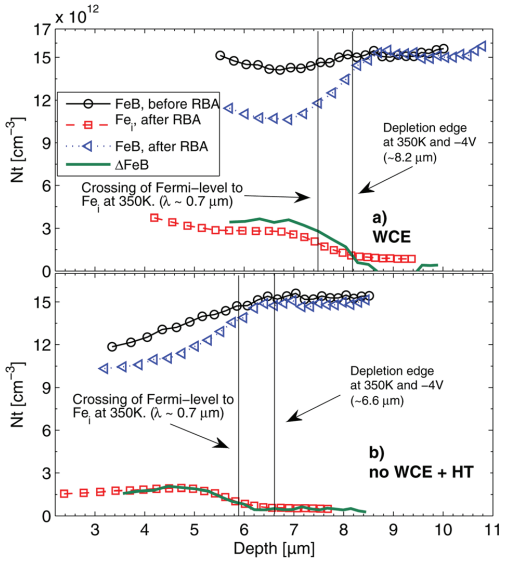

FIG. 3. (Color online) Defect concentration vs depth profile for Fe-B and Fe_i measured on (a) samples with WCE and (b) HT samples without WCE.

was recorded continuously during the RBA at 350 K. Due to the H re-distribution, a change in the capacitance takes place during RBA; it amounts, however, to only 0.3%, i.e., ~20 nm in the depletion edge depth and can be neglected.

The characteristics of a release of Fe_i by the Fermi-level effect are fulfilled in the HT samples where the influence of H is small. The depth profile in Fig. 3(b) shows that the increase of Fe_i occurs close to the charge state transition region (as highlighted by the vertical lines). However, in the WCE samples, a significant release of Fe_i can be observed not only in the region with Fe_i^0 but also in the part of the depletion region where Fe_i^+ exists. Moreover, the concentration of released Fe_i in the depletion region is higher by a factor of 1.5-2 in the WCE sample as compared to the HT sample. This demonstrates the significance of the mechanism, where Fe_i is released due to a direct dissociation of Fe-B promoted by H: $\text{Fe-B} + \text{H} \rightarrow \text{B-H} + \text{Fe}_i$.

It may be argued that Fe_i released close to the surface has in-diffused to such an extent that it could account for the measured defect profiles. However, the gain in concentration of Fe_i as a function of depth agrees closely with the loss of in concentration of Fe-B, implying that no significant net diffusion has occurred in the measured region.

As mentioned in the introduction, an interaction of H with Fe^0,[9] may be expected in the depletion region. However, based on our quantitative observations, we can not confirm formation of Fe-H complexes under the present experimental conditions; indeed, if hydrogen is to passivate Fe_i or Fe-B, a dissimilar concentration change between the two defects should occur. In addition, no new level in the vicinity of 0.3–0.4 eV above E_V, predicted for a donor state of the Fe-H pair, is observed. Thus, no evidence for passivation of Fe_i or Fe-B by H is obtained.

In conclusion, hydrogen has been incorporated into iron-contaminated boron-doped Cz-Si and demonstrated to interact with the Fe-B pair. By monitoring the absolute concentration of Fe-B and Fe_i versus depth before and after RBA, strong evidence of hydrogen-induced dissociation of the Fe-B pair into Fe_i and B-H are found confirming previous tentative experimental findings and recent theoretical predictions. In addition, no detectable passivation of Fe_i by hydrogen is observed.

This work was funded by the Norwegian Research Council through the project "Hydrogen in solar-grade p-type Si (HydSil)" within RENERGI program.

[1]A. A. Istratov, H. Hieslmair, and E. R. Weber, Appl. Phys. A **70**, 489 (2000), and references therein.
[2]M. Aoki, A. Hara, and A. Ohsawa, Jpn. J. Appl. Phys. **30**, 3580 (1991).
[3]M. Kouketsu and S. Isomae, J. Appl. Phys. **80**, 1485 (1996).
[4]A. Azzizi, L. J. Geerligs, and D. Macdonald, in *Proc. 19th Europ. PVSEC, Paris*, (2004), p. 1021, http://www.ecn.nl/publications/Default.aspx.
[5]M. D. Pickett and T. Buonassisi, Appl. Phys. Lett. **92**, 122103 (2008).
[6]E. B. Yakimov and A. L. Parakhonsky, Solid State Phenom. **57–8**, 383 (1997).
[7]O. Feklisova, A. Parakhonsky, E. Yakimov, and J. Weber, Mater. Sci. Eng., B **71**, 268 (2000).
[8]L. C. Kimerling and J. L. Benton, Physica B & C **116**, 297 (1983).
[9]M. Sanati, N. G. Szwacki, and S. K. Estreicher, Phys. Rev. B **76**, 125204 (2007).
[10]A. A. Istratov, H. Hielsmair, and E. R. Weber, Appl. Phys. A **69**, 13 (1999), and references therein.
[11]S. J. Pearton, J. W. Corbett, and M. Stavola, *Hydrogen in Crystalline Semiconductors* (Springer, Berlin, 1992).
[12]M. W. Horn, J. M. Heddleson, and S. J. Fonash, Appl. Phys. Lett. **51**, 490 (1987).
[13]T. Zundel and J. Weber, Phys. Rev. B **39**, 13549 (1989).
[14]C. H. Seager and R. A. Anderson, Appl. Phys. Lett. **59**, 585 (1991).
[15]P. Blood and J. W. Orton, *The Electrical Characterization of Semiconductors: Majority Carrier and Electron States* (Academic, San Diego, 1992).

IV

V

Divacancy-iron complexes in silicon

C. K. Tang,[1, a)] L. Vines,[1] V. P. Markevich,[2] B. G. Svensson,[1] and E. V. Monakhov[1]

[1)] *University of Oslo, Physics department/Center for Materials science and Nanotechnology, P.O. Box 1048 Blindern, N-0316 Oslo, Norway*

[2)] *Univ Manchester, Sch Elect & Elect Engn, Photon Sci Inst, Manchester M13 9PL, Lancs, England*

(Dated: 17 September 2012)

Iron and irradiation-induced defects have been investigated in p-type float-zone silicon after MeV electron-irradiation using deep level transient spectroscopy. Isochronal annealing (30 min) was performed up to 250°C, and three distinctive energy levels are observed in the Fe-contaminated samples with positions of 0.25, 0.29 and 0.34 eV above the valence band edge, respectively. The two latter ones are found to accompany the change in concentration of the divacancy center (V_2) during the isochronal annealing which suggests an interaction between Fe and V_2.

[a)]Electronic mail: c.k.tang@smn.uio.no (C. K. Tang)

I. INTRODUCTION

Iron is well-known for its detrimental effects on the performance of silicon solar cells and integrated circuits.[1] Solar cells based on p-type silicon can be significantly improved by gettering during a phosphorus in-diffusion step which accumulates Fe close to the surface and reducing its concentration in the bulk. Although this process is commonly employed, the underlying mechanism of the gettering of Fe is not fully understood. Furthermore, solar cells receiving the phosphorus gettering may still exhibit light-induced degradation with degradation characteristics of Fe contamination[2].

To further improve the gettering efficiency of Fe, it is important to understand the underlying mechanism and the defects formed during the gettering. Recently, it is shown that the major contribution of Fe gettering does not occur by the formation of a phosphorus-iron complex, where intentionally introduced Fe is gettered with a similar concentration versus depth profile regardless of the phosphorus depth profile.[3] In Ref.3, propose a mechanism involving oxygen and vacancies, injected during the phosphorus in-diffusion, was proposed.

Indeed, a reaction between the vacancy-oxygen complex and Fe have been reported in n-type silicon by You[4], using deep level transient spectroscopy (DLTS), and the defect was shown to be stable up to 300°C. The disappearance of the DLTS signal was suggested to be caused by the formation of a more stable complex, presumably substitutional Fe and interstitial oxygen. Furthermore, although not discussed in Ref.[4], the divacancy center (V_2) decreases in concentration after annealing at 80°C for 2.5h, suggesting a reaction between V_2 and Fe. This is also addressed by Komarov,[5] who investigated reactions between irradiation-induced defects with residual impurities in n-type silicon. Komarov observed the appearance of a hole trap at 0.184 eV above the valence band edge (E_V) after annealing at 150°C which

remained stable at 400°C. Tentatively, this defect was assigned to FeV_2, with the basic argumentation that Fe was present in the samples.

Theoretical calculations have recently been reported on the interaction between irradiation-induced defect and Fe.[6] The calculations predict two stable complexes between V_2 and Fe_i. The one with the lowest total energy is labelled as VFeV, where the Fe is situated half way between two vacancies. This configuration has a single acceptor level at E_V+0.38 eV (E_C-0.73 eV, where E_C is the conduction band edge) and a double acceptor level at E_C-0.55 eV. The other configuration is FeV_2 which has one donor level at E_V+0.25 eV and one acceptor level at E_V+0.36 eV (E_C-0.75 eV).

Recently, we have investigated the interaction between Fe and proton-irradiation-induced defects in p-type silicon using DLTS after isochronal annealing.[7] Several Fe-related defects were observed, and one appeared after 150°C with an energy level position of E_V+0.28 eV, labelled as H(0.28). Based on the evolution of the concentrations of H(0.28) and V_2, H(0.28) was tentatively assigned as a divacancy-Fe complex, although, the involvement of hydrogen (arising from proton-implantation) could not be ruled out.

In this study, Fe-contaminated and Fe-lean float-zone (Fz) p-type silicon samples have been irradiated by electrons and investigated for possible reactions of Fe with irradiation-induced defects. Several deep level defects are observed exclusively in the Fe-contaminated samples after annealing above 125°C, and two of these involve possibly V_2.

II. EXPERIMENT

Samples were cut from Fz boron-doped silicon with doping concentration of 2×10^{14}cm^{-3}, as confirmed by capacitance-voltage (CV) measurements. Dry oxidation was performed at 1000°C for 8h after an HF-dip, and circular holes of 2 mm in diameter were opened at

the frontside using photolitography for the preparation of a pn-junction. Phosphorus was implanted at the frontside with an energy and dose of 36 keV and 1×10^{14}cm^{-2}, respectively. Thereafter, Fe was implanted at the rearside with energy and dose of 700 keV and 1×10^{14}cm^{-2}, respectively. After the implantation, the samples were heat treated at 875°C for 1h to activate the n^+-layer and to diffuse Fe to the frontside of the sample.[8]

Aluminium contacts of 1 mm in diameter were deposited onto the n^+-layer of the pn-junction, and Ohmic contacts were formed at the rearside by applying silver-paste. The samples were electrically characterized using CV-measurement and DLTS. For DLTS, six rate-windows were used ranging from $(20\text{ms})^{-1}$ to $(640\text{ms})^{-1}$ and the signals were typically extracted by the GS4 weighting function[9]. The reverse and pulse bias voltages were 4.5 and -4.5V, respectively.

After initial DLTS measurements, which confirmed that only the Fe-contaminated samples (and not the control ones) contained the Fe-B pair and/or interstitial Fe (Fe_i) while other centers were below the detection limit, electron-irradiation was performed with an energy of 4 MeV and a dose of 2×10^{14}cm^{-2}. The reference samples, which were based on Al Schottky barrier contact and not intentionally contaminated with Fe, received the same electron-irradiation. The electron-irradiated samples were stored for three weeks at room temperature before commencing characterization and isochronal annealing (30 min) from 125 to 250°C with an interval of 25°C.

III. RESULTS AND DISCUSSION

Figure 1 shows the DLTS spectra of Fe-contaminated (Fig.1a) and reference (Fig.1b) samples in the as-implanted state and after annealing at 150, 200 and 250°C. The ordinate in the temperature interval of 90 to 160K has been enhanced by a factor 8 for clarity. Fo-

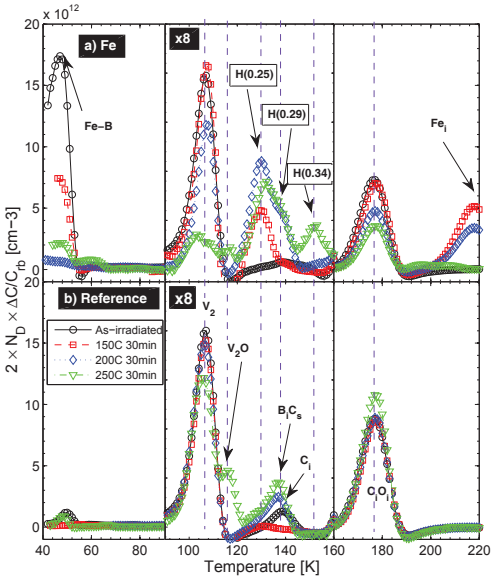

FIG. 1. Spectra of DLTS measurements, with GS4 weighting function, on electron-irradiated Fe-contaminated and reference samples before and after annealing at 150, 200 and 250°C for 30 min. Three distinctive peaks, H(0.25), H(0.29) and H(0.34), are only found in the Fe-contaminated samples. These spectra are extracted from rate-window of $(640\text{ms})^{-1}$.

cusing on the as-implanted samples, prominent irradiation-induced defects can be observed both in the reference and the Fe-contaminated samples, such as the V_2[10–12] and the interstitial carbon-interstitial oxygen pair (C_iO_i)[11,13] with the respective energy level positions of 0.18 eV and 0.35 eV above E_V. Small amount of interstitial carbon (C_i)[13] can also be observed at 139K ($\sim E_V$+0.30 eV), but it becomes negligible after annealing above room temperature.

In the Fe-contaminated samples (Fig.1a), the Fe-B pair is observed at 47K ($\sim E_V$+0.10 eV) and concentration of $1.7\times10^{13}\text{cm}^{-3}$. Fe-B can dissociate into Fe_i in a reversible reaction by heat treatment, illumination or by minority carrier injection.[8,14] Fe_i occurs at E_V+0.40 eV

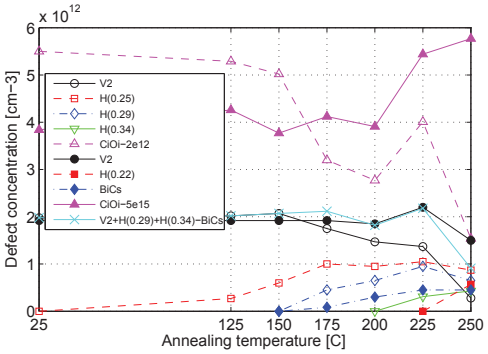

FIG. 2. Evolution of the defect concentrations in Fe-contaminated (open symbol) and reference samples (filled symbol) to subsequent annealings of 30 min. Data from as-irradiated samples are plotted at annealing temperature of 25°C. "V2+H(0.29)+H(0.34)-BiCs" is a result from adding the concentration of V_2, H(0.29) and H(0.34) in the Fe-contaminated samples and subtracting B_iC_s from the reference samples.

and can be readily observed in Fig.1 at 218K after annealing at 150°C. It should be mentioned that the sum of the concentration of the Fe-B pair and the Fe_i decreases by subsequent annealing. Fe_i is highly mobile and the decrease may be explained by migration to the surface, or reactions with other defects such as the irradiation-induced ones.

Figure 2 summarises the concentration of the observed defects levels after subsequent annealings (30 min). The data for C_iO_i have been subtracted with 2×10^{12} and 5×10^{12}cm^{-3} for the Fe-contaminated and the reference samples, respectively, to increase the clarity of the figure. In the reference samples, the concentration of C_iO_i is stable above 250°C, in accordance with the dissociation energy of ∼2.0 eV of the complex.[15] For the V_2, a slight decrease takes place after 250°C, which can be associated with the formation of V_2O[16]; indeed, a peak appears at 116K in Fig.1, with a position of E_V+0.22 eV and an apparent capture cross-section of 1×10^{-15}cm^2, in accordance with previous observations.[16,17] For the

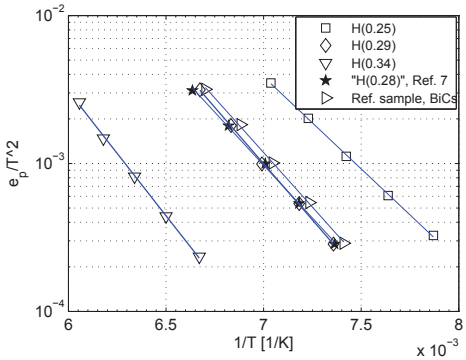

FIG. 3. Arrhenius plot of the three distinctive deep levels in Fe-contaminated samples and two additional set of data for comparison. The data points for H(0.29) are extracted from the simulated DLTS spectra, partially shown in Fig.4, and compared with those of B_iC_s in the reference samples and from Ref.[7].

Fe-contaminated samples, however, a different trend occurs for V_2 and C_iO_i. Both defects exhibit a reduction in concentration already after 150°C, with the exception of a sudden increase of C_iO_i at 225°C. Hence, a different and more complex annealing behavior of the irradiation-induced defects is unveiled due to the presence of Feas will be discussed in more detail later.

Three distinctive peaks are exclusively observed in the Fe-contaminated samples at 130, 136 and 153K with the corresponding labels of H(0.25), H(0.29) and H(0.34). The Arrhenius plots of these levels are shown in Fig.3, and the extracted energy level positions are 0.25, 0.29 and 0.34 eV above E_V with apparent capture cross-sections of 1×10^{-14}, 9×10^{-15} and 2×10^{-14}cm^2, respectively. The data points for H(0.25) and H(0.29) are extracted after simulating the DLTS spectra, as displayed in Fig.4 (only two rate windows are displayed for clarity.)

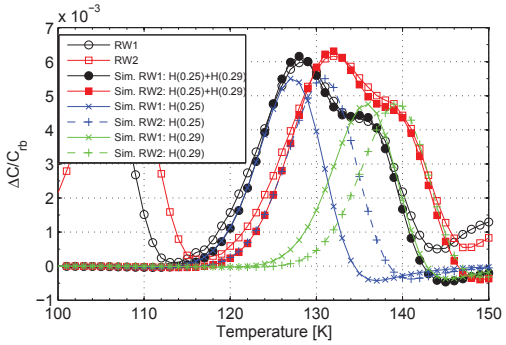

FIG. 4. Simulated (Sim.) DLTS spectra for the H(0.25) and H(0.29) peaks between 120 to 150K for rate window 1 (RW1) of $(640\text{ms})^{-1}$ and rate window 2 (RW2) of $(320\text{ms})^{-1}$.

Figure 3 contains two additional set of data; one set is extracted from the peak at 135K in the reference samples after annealing above 150°C. The Arrhenius plot for the reference sample reveals an energy level position and an apparent capture cross-section of E_V+0.29 eV and $2\times10^{14}\text{cm}^2$, respectively, and the level is identified as the interstitial boron-substitutional carbon (B_iC_s).[18] Based on the similar properties of B_iC_s and H(0.29), it may be tempting to attribute H(0.29) solely as B_iC_s. However, in addition to the larger concentration in the Fe-contaminated samples than in the reference samples (Fig.2), the concentration versus depth profiles differ significantly, as shown in Fig.5. B_iC_s remains close to constant as a function of depth in the reference sample, as expected in MeV electron-irradiated samples, while H(0.29) exhibits a significant increase in concentration towards the bulk. This implies that H(0.29) is not primarily due to B_iC_s, but forms when an impurity diffuses from the back towards the surface. Since Fe is highly mobile at elevated temperatures, it is one main candidate to be involved in H(0.29). The second set added in Fig.3 is taken from Ref.[7] and is the data for the tentatively assigned divacancy-Fe complex, H(0.28). A close agreement is found between the H(0.29) and H(0.28) data sets

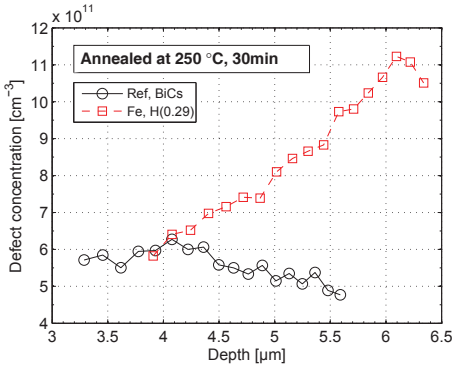

FIG. 5. Concentration versus depth profiles of H(0.29) in the Fe-contaminated samples and the B_iC_s in the reference samples.

If H(0.29) is assumed to be the donor state of FeV_2, as predicted in Ref.[6], a second signal at E_V+0.36 eV with similar amplitude is expected in the DLTS-measurement. However, a peak with the suggested energy level position has a strong overlap with the dominating C_iO_i and can not be readily resolved.

H(0.34) in this work has a position close to that calculated for the single acceptor of VFeV, in Ref.[6]. Furthermore, H(0.34) is formed after annealing at 225°C and increases further at 250°C which indicates a rather stable defect, consistent with that predicted VFeV.

If H(0.34) and H(0.29) are due to Fe-related complexes invoking V_2, a correlation in the defect concentration versus annealing temperature is a necessary condition. Assuming that B_iC_s in the Fe-contaminated samples has the same concentration as in the reference samples, the sum of V_2, H(0.29) and H(0.34) (Fe-contaminated samples) minus B_iC_s (reference samples) is depicted in Fig.2 (labelled as "V2+H(0.29)+H(0.34)-BiCs"). This curve follows closely the concentration of V_2 in the reference samples below 250°C. Above 250°C, other reactions start to dominate the annealing of V_2, like formation of V_2O.[16,17] From these considerations, it is suggested that H(0.29) and H(0.34) are caused by complexes formed

through reactions between mobile Fe and V_2.

H(0.25) appears at 125°C and remains essentially stable at temperatures above 175°C (Fig.2). Although its concentration correlates with the loss of C_iO_i below 175°C, suggesting a relation to C_iO_i, the pattern is not unambiguous above 175°C. One may speculate that a further (higher order) reaction between Fe and C_iO_i passivates the H(0.25) complex which will account for the decrease in the concentration of C_iO_i and possibly also the saturation of H(0.25). However, the literature on interaction between Fe and C_iO_i is scarce and further investigations should be persued; for instance with isothermal annealing including reverse biasing.

IV. CONCLUSION

Boron-doped and Fe-contaminated Fz silicon samples have been electron-irradiated and investigated for Fe-related defects using DLTS after isochronal annealings up to 250°C. Three distinct deep levels are exclusively revealed in the Fe-contaminated samples after annealing. The concentration of two ones, H(0.29) and H(0.34), accompany the loss in concentration of V_2, suggesting an interaction between mobile Fe and V_2, in full accordance with previous theoretical predictions in the literature.

ACKNOWLEDGMENTS

This work was funded by the Norwegian Research Council through the project “Hydrogen in solar-grade p-type Si (HydSil)” within the RENERGI program.

REFERENCES

[1]A. A. Istratov, H. Hielsmair, and E. R. Weber, Appl. Phys. A, **70**, 489 (2000), **and references therein**.

[2]J. H. Reiss, R. R. King, and K. W. Mitchell, Appl. Phys. Lett., **68**, 3302 (2008).

[3]M. Syre, S. Karazhanov, B. R. Olaisen, A. Holt, and B. G. Svensson, J. Appl. Phys., **110**, 024912 (2011).

[4]Z.-P. You, M. Gong, J.-Y. Chen, and J. W. Corbett, J. Appl. Phys., **63**, 324 (1987).

[5]B. A. Komarov, Semiconductors, **38**, 1079 (2004).

[6]S. K. Estreicher, M. Sanati, and N. G. Szwacki, Phys. Rev. B, **77**, 125214 (2008).

[7]C. K. Tang, L. Vines, B. G. Svensson, and E. V. Monakhov, "Deep level transient spectroscopy on proton-irradiated Fe-contaminated p-type silicon," Phys. Status Solidi C (Accepted in 2012).

[8]C. K. Tang, L. Vines, B. G. Svensson, and E. V. Monakhov, Appl. Phys. Lett., **99**, 052106 (2011).

[9]A. A. Istratov, J. Appl. Phys., **82**, 2965 (1997).

[10]B. G. Svensson, A. Hallén, J. H. Svensson, and J. W. Corbett, Phys. Rev. B, **43**, 2292 (1991).

[11]H. Malmbekk, L. Vines, E. V. Monakhov, and B. G. Svensson, Solid State Phenom., **178-179**, 192 (2011).

[12]P. M. Mooney, L. J. Cheng, M. Süli, J. D. Gerson, and J. W. Corbett, Phys. Rev. B, **15**, 3836 (1977).

[13]J. Lalita, N. Keskitalo, A. Hallén, C. Jagadish, and B. G. Svensson, Nucl. Instrum. Meth. B, **120**, 27 (1996).

[14]A. A. Istratov, H. Hielsmair, and E. R. Weber, Appl. Phys. A, **69**, 13 (1999), **and references therein**.

[15]B. G. Svensson and J. L. Lindström, Phys. stat. sol A, **95**, 537 (1986).

[16]M. Mikelsen, E. V. Monakhov, G. Alfieri, B. S. Avset, J. Härkönen, and B. G. Svensson, J. Phys. Condens. Mat., **17**, S2247 (2005).

[17]M.-A. Trauwaert, J. Vanhellemont, H. E. Maes, A.-M. V. Bavel, G. Langouche, and P. Clauws, Appl. Phys. Lett., **66**, 3065 (1995).

[18]O. J. Drevinsky, C. E. Caefer, S. P. Tobin, J. C. Mikkelsen, JR., and L. C. Kimerling, in *MRS Proceedings 1987*, Vol. 104 (1987) p. 167.

VI